Finding the concealed section of the Whakatane Fault in the Whakatane Township with a shear wave land streamer system: A seismic surveying report

U. Polom
C. Mueller
A. Nicol
P. Villamor
R.M. Langridge
J.G. Begg

GNS Science Report 2016/41
August 2016

GNS SCIENCE
TE PŪ AO

DISCLAIMER

The Institute of Geological and Nuclear Sciences Limited (GNS Science) and its funders give no warranties of any kind concerning the accuracy, completeness, timeliness or fitness for purpose of the contents of this report. GNS Science accepts no responsibility for any actions taken based on, or reliance placed on the contents of this report and GNS Science and its funders exclude to the full extent permitted by law liability for any loss, damage or expense, direct or indirect, and however caused, whether through negligence or otherwise, resulting from any person's or organisation's use of, or reliance on, the contents of this report.

BIBLIOGRAPHIC REFERENCE

Polom, U.; Mueller, C.; Nicol, A., Villamor, P., Langridge, R.M.; Begg, J.G. 2016. Finding the concealed section of the Whakatane Fault in the Whakatane Township with a shear wave land streamer system: A seismic surveying report. *GNS Science Report* 2016/41. 41 p.

U. Polom, LIAG, Stilleweg 2, 30655 Hannover, Germany

C. Mueller, GNS Science, PO Box 30368, Lower Hutt 5040, New Zealand

A. Nicol, University of Canterbury, Private Bag 4800, Christchurch 8140, New Zealand

P. Villamor, GNS Science, PO Box 30368, Lower Hutt 5040, New Zealand

R.M. Langridge, GNS Science, PO Box 30368, Lower Hutt 5040, New Zealand

J.G. Begg, GNS Science, PO Box 30368, Lower Hutt 5040, New Zealand

www.gns.cri.nz

ISSN 1177-2425 (Print)
ISSN 2350-3424 (Online)
ISBN 978-0-947510-75-6 (Print)
ISBN 978-0-947510-76-3 (Online)

CONTENTS

FIGURES

TABLES

ABSTRACT

The principal objective of the presented study was to evaluate the usefulness of high-resolution shear wave seismic reflection profiling using a land streamer to locate buried faults in urban areas of New Zealand. A secondary objective was to locate the Whakatane Fault. In a calibration survey the method was first tested over a surface trace of the Edgecumbe Fault 30 km south-west of Whakatane township, that ruptured during the 1987 Mw 6.3 Edgecumbe Earthquake. This survey helped gain an understanding of the shear wave propagation characteristics across an active fault in the sediments of the area. These comprise pumiceous material from the Taupo Volcanic Zone redeposited in a Holocene marine and fluvial environment. Having established the characteristics of shear wave seismic images in a green field location, the main survey was conducted within the Whakatane township.

In total, 11 high quality profiles of 5.7 km total length were acquired, showing concealed displacements in sediments to a depth of 100 m. Normal fault displacements of up to 15 m are visible in depths from 20 to 40 m and deeper structures show displacements of up to 20 m. The technique proved useful for accurately defining the location of the Whakatane Fault beneath the township of Whakatane on several East/West profiles. Corroborative evidence for the location of the fault requires a drilling programme.

KEYWORDS

Land streamer survey, Whakatane Fault, concealed faults in urban environments

1.0 INTRODUCTION

The recent Mw 7.1 Darfield Earthquake produced rupture of the ground surface along the Greendale Fault, that was unknown prior to the earthquake (e.g., Quigley et al., 2010a, 2010b, 2012; Barrell et al., 2011; Van Dissen et al., 2011). Subsequent earthquakes in the Canterbury Earthquake Sequence occurred on other blind faults in the Christchurch area. Analysis of active faults incorporated into the National Seismic Hazard Model (NSHM) suggests that several thousands of these structures may be unidentified and have the potential to generate moderate to large magnitude earthquakes (i.e., magnitudes >5) (Nicol et al., 2011).

The database that underpins the NSHM mainly comprises active faults exposed at the surface and incorporates historical seismic data. In areas where the rates of surface processes exceed fault displacement rates, active faults may be difficult to observe at the ground surface. Geological mapping suggests that active faults pass beneath, or within 10 km of, many urban areas in New Zealand, including Auckland, Blenheim, Christchurch, Hastings/Napier, Nelson, Rotorua, Taupo, Wellington and Whakatane (e.g., Langridge et al., 2016). Mapping their exact location and assessing their seismic hazard is essential for planning future urban development and for emergency response and recovery.

The Canterbury earthquakes demonstrate that some of these hidden faults could pose a significant risk to New Zealand society, particularly where they are located beneath or close to urban areas. The Royal Commission for the Canterbury Earthquakes recommended that "Research continues into the location of active faults near Christchurch and other population centres in New Zealand, to build as complete a picture as possible for cities and major towns" (Canterbury Earthquakes Royal Commission, 2012). While the international nuclear industry has developed methods for locating potential active faults, and assessing their hazards, these methods tend to be very complex and expensive prohibiting their use in urban planning. In New Zealand no method has been established for routinely locating and assessing the earthquake hazard posed by concealed active faults.

Seismic reflection profiles designed to image shallow (e.g., 500 m) stratigraphy and structure offers potential for locating concealed active faults. The land streamer source and receiver technology applied in this study is specially designed for use on roads and in built-up areas. The use of shear waves (S-waves) in shallow seismic reflection surveying provides significantly higher resolution compared to the commonly applied compressional waves (P-waves; e.g., in hydrocarbon seismic reflection exploration). At the groundwater table in the subsurface, P-wave propagation velocity escalates above 1500 m/s, usually leading to an elongation of the wavelength to greater than 15 m assuming a sophisticated central signal frequency of 100 Hz. Since shear waves are not affected by pore fluid and propagate in the soil matrix only, the propagation velocity in soil remains around 150 m/s above and below the groundwater table. Even assuming a lower central signal frequency of 50 Hz than that commonly used for P-wave analysis, the wavelength reduces to 3 m, resulting in a potential improvement in resolution of five times. In water saturated soft sediments resolution can be improved by a factor greater than 10. Furthermore, the shear wave vibratory source gradually releases its energy into the ground reducing risk of ground surface damage that can occur in conjunction with impulse type sources.

This study aims to address the recommendation of the Royal Commission (Canterbury Earthquakes Royal Commission, 2012) by exploring economic ways of locating active faults beneath cities using seismic reflection technology. The principal objective is to test the usefulness of high-resolution shear wave seismic reflection profiling using a land streamer to locate buried faults. We tested its use in locating the Whakatane Fault within the urban area of Whakatane, using the land streamer developed by Leibniz Institute for Applied Geophysics (LIAG). To test the resolution and style of fault deformation we could expect in the soft, young sediments beneath Whakatane, we undertook preliminary seismic reflection surveys across the Edgecumbe Fault, the location and style of deformation of which is well known due to carefully documented work following its surface rupture in 1987 (e.g., Beanland et al., 1989).

2.0 THE WHAKATANE AND EDGECUMBE FAULTS

This study focuses on the Edgecumbe and Whakatane faults (Figure 2.1). Paleoseismic studies indicate that the faults are active and capable of generating future surface-rupturing earthquakes (Beanland et al., 1989; Beanland, 1995; Mouslopoulou et al., 2008, 2009; Begg and Mouslopoulou, 2010). These faults were selected for this study because: a) Materials near the Edgecumbe Fault are similar to those beneath Whakatane, and have been subject to a well-documented historical surface displacement; and b) The Whakatane urban area hosts a buried active fault in a region compatible with investigation using low impact seismic acquisition techniques.

The seismic reflection profiles obtained across the green fields site at the Edgecumbe Fault are expected to aid interpretation of tectonic deformation of the profiles obtained within the Whakatane township.

While displacement across the Whakatane Fault is expected to be oblique, that is with normal and strike-slip components of motion (Mouslopoulou 2006; Mouslopoulou et al., 2009), Edgecumbe Fault displacement is purely normal. We expect that deformation associated with the vertical component of the Whakatane Fault may resemble that of the Edgecumbe Fault.

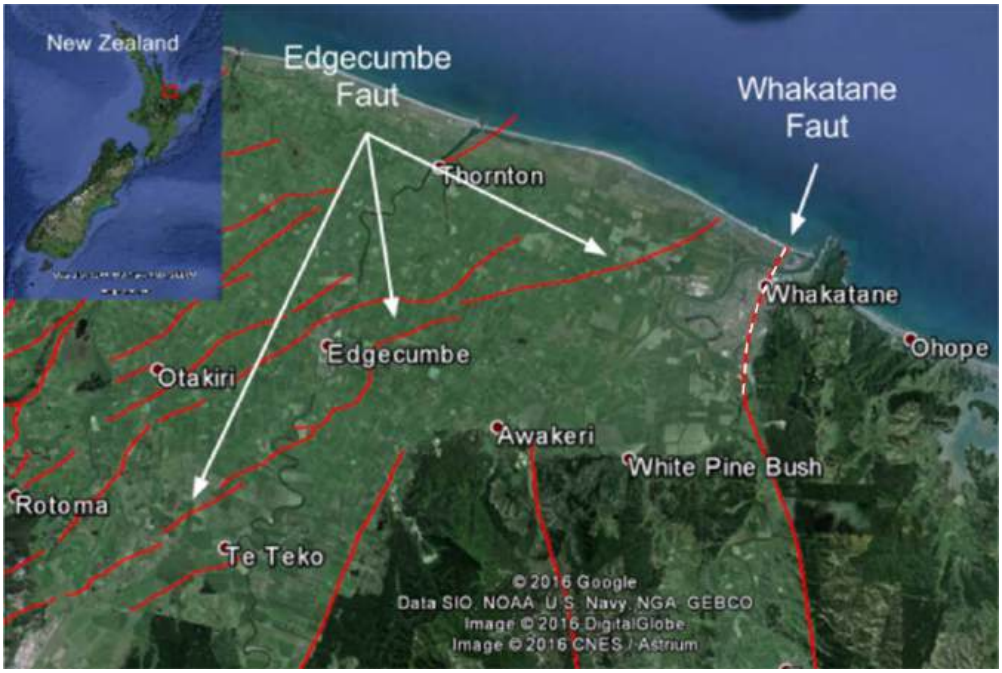

Figure 2.1 Location of the Edgecumbe and Whakatane Faults as indicated in the New Zealand Active Faults Database (Langridge et al., 2016). The dashed part of the Whakatane Fault line indicates where the location is currently only inferred.

The Whakatane Fault forms part of the North Island Fault System (NIFS; also known as the North Island Dextral Fault Belt; Figure 2.1), which can be traced almost continuously for nearly 400 km from the southern North Island to the Bay of Plenty coastline (Beanland, 1995; Mouslopoulou et al., 2007). The fault has been mapped to the outskirts of Whakatane (e.g., Mouslopoulou et al., 2009). South of Whakatane (Ruatoki, not shown on the map in Figure 2.1) it displaces Late Holocene alluvium (Mouslopoulou et al., 2009). In the urban area the near-surface deposits of Late Holocene alluvium and beach ridges are not unambiguously displaced by the fault. Due to the lack of a clear surface trace the precise location of the fault was not known in the urban area prior to the present study[1]. In the Whakatane region immediately south of the city the fault strikes NNW and dips steeply to the west (60-70°) (Nairn et al., 1989; Beanland, 1995; Woodward-Clyde, 1998; Mouslopoulou et al., 2007, 2009). Within 10 km of the coastline, the fault accommodates approximately equal rates of normal dip-slip (1.5±0.5 mm/yr) and right-lateral strike-slip (1.1±0.5 mm/yr; Mouslopoulou 2006 and Mouslopoulou et al., 2009). Normal displacements are indicated by numerous prominent scarps that are down to the west, by a normal slip in a fault trench and by a westward throw of, at least, 500 m on the top of the basement inferred from modelling of a gravity survey (Mouslopoulou et al., 2008). The Whakatane Fault proximal to Whakatane has accommodated at least three surface-rupturing prehistoric earthquakes over the last 10 kyr (Mouslopoulou et al., 2009). The youngest of these events probably occurred within the last 800 yrs while the older two earthquakes most likely ruptured the fault between 5 and 10 kyr BP. The average net slip at the ground surface during these earthquakes is estimated to be about 3 m (Mouslopoulou et al., 2009). Near–surface deformation associated with the Whakatane Fault has been exposed in paleoseismic trenches south of the city (Beanland, 1995; Mouslopoulou et al., 2009). Displacement across the fault is expressed as a single, sharp oblique (normal and strike-slip) fault or a series of subparallel fault splays within a width of 2-3 m.

The Edgecumbe Fault (Figure 2.1) is a normal fault that is a key element of the Taupo Rift which extends through the central North Island and offshore into the Bay of Plenty (Rowland and Sibson, 2001; Villamor and Berryman, 2001; Nairn, 2002; Lamarche et al., 2006). The fault strikes north to northeast and dips moderately to the west at 60-70°. It displaces the surface of the Rangitikei Plains which are locally dominated by alluvial deposits <1.7 kyr in age (Begg and Mouslopoulou, 2010). The active fault trace forms a scarp up to 3.8 m high along a distance of about 10 km (Beanland et al., 1989; Nairn and Beanland, 1989; Mouslopoulou et al., 2008; Begg and Mouslopoulou, 2010). Seismic reflection profiles and gravity modelling suggest that the fault displaces the top of Mesozoic basement by 2-2.5 km and probably extends laterally beyond the active surface trace. These seismic data suggest the Edgecumbe Fault has an average slip rate of about 4 mm/yr over the last 300 kyr (Mouslopoulou et al., 2008). At Edgecumbe the fault has ruptured the ground surface at least three times in the last ~1.7 kyr (Beanland et al., 1989). The most recent of these was in the 1987 M_w 6.5 Edgecumbe Earthquake which produced the majority of the scarp height observed today (Beanland et al., 1989). The Edgecumbe Earthquake is the youngest surface-rupturing earthquake in the Taupo Rift.

[1] Begg & Mouslopoulou (2007), in the course of their Rangitaiki Plains work located a feature within Whakatane itself that they interpreted to represent the Whakatane Fault (see digital data). This resulted in the study of the Beetham et al., 2010 that independently tested the validity of this interpretation using gravity data. The conclusions from the latter study suggested that the interpretation was not supported by the new data.

Deformation of the ground surface along the Edgecumbe Fault during the 1987 earthquake was expressed in different ways; broad scarps, sharp narrow scarps and extensional fissures (Beanland et al., 1989). Paleoseismic trenches undertaken shortly after the event exposed the deformation of the upper ~ 2m metres of sediments (water table was high impeding deeper excavations) (Beanland et al., 1989). The deformation consistent with the morphology of the surface scarps. Broad monoclines were found in areas where the surface fault scarps were broad, often associated with minor discrete fault displacement. Other trenches exposed sharp discrete strata displaced across a well-defined normal fault or series of fault splays. Large extensional fissures frequently formed in association with monoclines and faults. While these features are likely superficial (e.g., < 10 m depth), they are important in interpreting tectonic deformation in deeper parts of the alluvial setting of the Rangitikei Plains from the seismic reflection profiles.

This page is intentionally left blank.

3.0 SEISMIC ACQUISITION METHODOLOGY

The survey was carried out using the vibroseis method (Crawford et al., 1960) originally developed for hydrocarbon exploration. Instead of using impulse sources such as a hammer impact or explosives to generate a seismic signal, highly defined and coded vibrations (so called 'sweeps') are transmitted into an elastic wave in the ground (Figure 3.1). The advantages of this principle are to stretch the signal energy in time, to reduce the initial forces to prevent damages, and to control the signal frequency range. Furthermore, it enables start timing in high-precision and a perfect reproducibility. The emitted source signal propagates in the subsurface in the same manner like an impulse signal and is recorded using the same type of equipment. After recording, the coded signal is decoded by a computer algorithm (Vibroseis Correlation process) and imaged in a similar manner to the impulse signal.

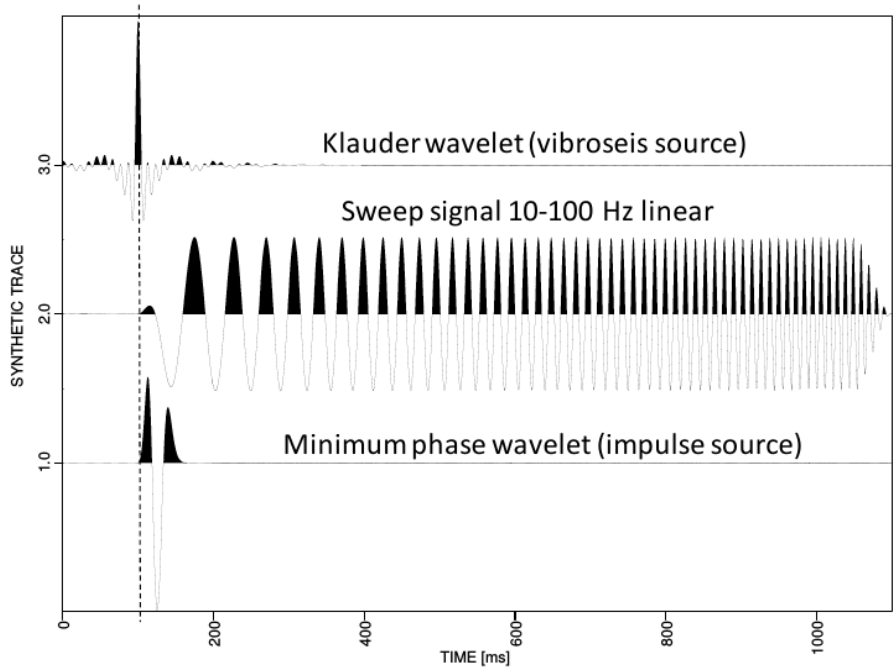

Figure 3.1 Top: the result of the Vibroseis Correlation process applied to the Vibroseis Sweep signal shown in the middle. Due to the two-sided symmetrical signal form with respect to the reference time 100 ms this signal is called a Klauder wavelet, a non-causal wavelet type because it starts prior to the reference time. Bottom: the typical form of an impulse source signal called minimum phase wavelet, which is causal with respect to the reference time, which means all energy occurs up after 'ignition'.

In hydrocarbon seismic exploration compression waves (P-waves) are most commonly used. The second body wave type that exists in solids, the so called shear wave (S-wave), is always slower than the P wave and is not affected by pore fluid, because it depends on the shear modulus of the material only, which is zero for fluids. Details of the elastic wave theory are described by Aki and Richards (1980). S-wave exploration is not common in hydrocarbon seismic exploration because it enables only poor information for the main target of the hydrocarbon industry, the fluid oil or gas in the pore space. In the shallow subsurface of unconsolidated, fluid-saturated sediments, the ratio between P- and S-wave velocities may rise up to a factor of 12 or more. Therefore in such an environment, shear waves enable much shorter wavelengths and are therefore able to detect details of buried structures in considerably higher resolution (Ghose et al., 1996). Since 2002 the Leibniz Institute for Applied Geophysics, Germany (LIAG) has been

involved in research and development using this specific wave type for shallow subsurface investigations. The development combines state-of-the-art vibration technology (Polom, 2005) together with modern seismic recording and data processing techniques, as used in the hydrocarbon industry. The technique enables high-resolution imaging of the shallow subsurface material to a depth of up to 100 m using a relatively small amount of equipment. The current state of development enables resolutions of up to 0.5 m vertical. Lateral resolution begins at 0.5 m close to the surface and, depending on the seismic velocities, diminishes linearly with depth (e.g., 2-3 m at about 20 m depth). A particular advantage of the equipment developed by LIAG is its design to operate on paved surfaces like asphalt roads or concrete, which means the system is well-tailored for deployment in urban areas.

4.0 SHEAR WAVE SEISMIC DATA ACQUISITION AT THE EDGECUMBE FAULT AND WHAKATANE SITES

Three seismic profiles were obtained across the Edgecumbe Fault in three different transects along the fault where the geomorphic fault scarp is clear but has differing heights. Profiles 1 and 2 are located in the middle of the mapped fault trace where the scarp is several meters high (3.4 and 3 m respectively), while profile 3 is in a section of the fault closer to the trace end which show less surface displacement (1m; Beanland et al., 1989: Figure 4.1). The Edgecumbe Fault survey was carried out to serve as a reference and calibration survey. The location of the fault is still visible in the landscape and the fault and the associated 1987 rupture is well studied, giving us an opportunity to understand the characteristics of seismic images across an active fault in a similar sedimentary sequence to that at Whakatane.

The aim in Whakatane was to locate the Whakatane Fault within the town where its precise location was unknown prior to this study. In Whakatane, E-W profiles across the strike of the fault were designed to include the likely location of the fault. The profiles cover most of the Whakatane residential area (Figure 4.1). An overview of the survey area is shown in Figure 4.1. The figure caption gives a reference to the names of the streets these profiles followed.

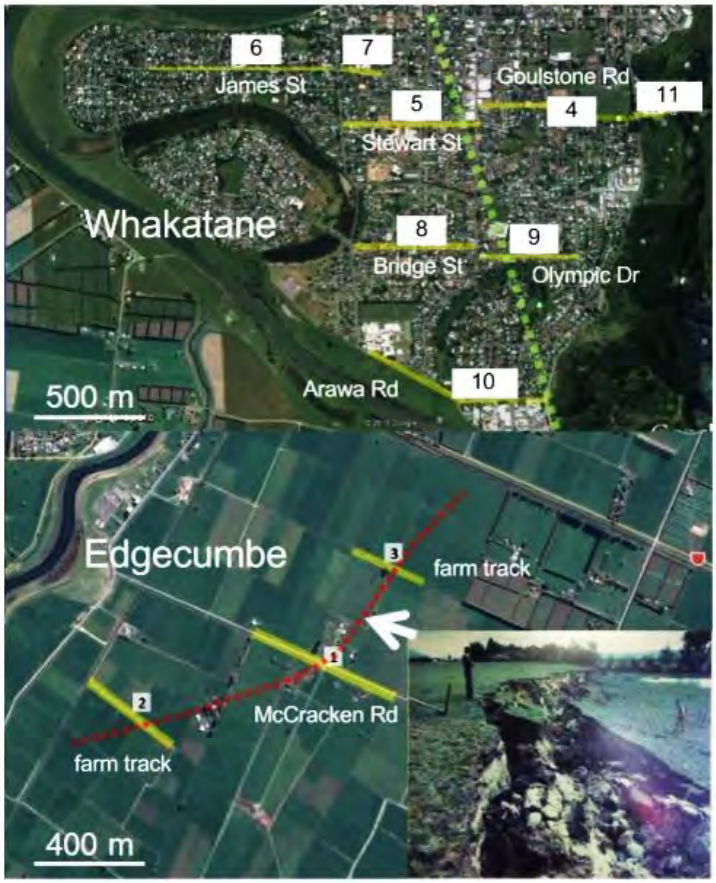

Figure 4.1 Overview of the survey area and seismic profiling map (yellow lines) at Edgecumbe (lower) and Whakatane (upper) survey sites. At Edgecumbe, the red dotted line marks the fault scarp of the 1987 rupture, the green dotted line marks the linear extrapolated Whakatane Fault trace from its known location south of the city. Street names: 1 - McCracken Rd, 2,3 - farm tracks, 4 - Goulstone Rd, 5 - Stewart St, 6,7 - James St, 8 - Bridge St, 9 - Olympic Dr, 10 - Arawa Rd, 11 - Gorge Rd.

4.1 DATA ACQUISITION AND FIELD PARTY

The field party consisted of 4 people with a support of two staff for traffic management.

The seismic recording parameters for the survey are shown in Table 4.1. Each seismic profile recorded was stored in the original non-correlated and unstacked version to enable noise reduction processing, if required, at a later date. Geodetic surveying of the seismic profiles was carried out with a handheld DGPS system. Parallel to data recording and storing, vibroseis correlation processing, digital filtering and scaling was applied to the data by the recording system. This allowed for data quality control and a rapid initial interpretation.

Table 4.1 Seismic acquisition parameters.

Seismic recording parameters **SH shear wave reflection seismic at Edgecumbe Fault and Whakatane sites 09.-23.02.2015**	
Recording system	Geometrics GEODE, 96 channels (Geometrics Inc., Tulsa OK, U.S.A.), 4 modules of 24 channels each, Pilot sweep on channel 96
Geophone type	Single geophone SM6-H 10 Hz (horizontal), SH configuration, mounted on a GEOSYM land streamer system
Receiver interval	1 m
Recording time	12 s (noncorrelated)
Sampling interval	1 ms
Recording filter	---
Polarity	SEG convention
File format Data storage type	SEG2 Unstacked, noncorrelated
Source	ELVIS version 6 SH shear wave vibrator, electrodynamic, wheelbarrow mounted
Source interval	4 m, on profile 10 partly 8 m
Source signal	20-80 Hz linear sweep, 10 s duration, 200 ms cos taper
Recording time after correlation	2 s
Vibration count/location	2 ([+Y] – [-Y] alternating vibrations)

Along a total profile length of 5.72 km and 13 Gb of seismic data were recorded. Initial data processing using VISTA 10.028 (GEDCO, Calgary, CA) reflection seismic processing software was carried out every day to give a timely overview and evaluation of the results. With this approach we were able to optimize the profiling schedule and profile tracks during the survey, depending on imaged subsurface structure. Nearly 30% of the initial acquisition plan was changed during the survey, mostly at the Whakatane site.

After initial parameter tests on profile 1, we decided to use a source signal with a frequency range of 20-80 Hz (2 octaves) and 10 s duration, since higher frequencies could hardly be observed in the subsurface response. Furthermore, highest resolution was of minor interest for the survey targets, in contrast to a sufficient penetration depth of at least 50 m. The chosen frequency range should also overcome the limitations caused by the relatively low shear-wave velocities of 50-250 m/s of the subsurface deposits. Due to the sufficient subsurface response we chose 4 m source interval to allow for fast profiling progress. This resulted in a mean CMP coverage of nearly 12-fold. Profiles 1-3 at the Edgecumbe site were acquired during daylight due to low traffic and environmental noise. Profiles 4-11 in Whakatane were acquired during night time hours between 10 pm and 5 am, to reduce traffic noise and increase safety. Also the noise level induced by wind was lower after sunset during the entire survey. For the most part of the survey we applied a variable split-spread geometry setup moving the source relative to geophone 24 to geophone 72 in a fixed streamer position. This allowed us to detect dipping structures in both profile directions, to improve the offset range for hyperbola analysis during the velocity analysis, and to minimize problems of geophone-to-ground coupling. After finishing this shooting pattern along the streamer, the streamer was shifted forward 48 m to start the next part of the survey.

4.2 DESCRIPTION OF THE TECHNICAL SETUP

4.2.1 The LIAG shear wave micro source system

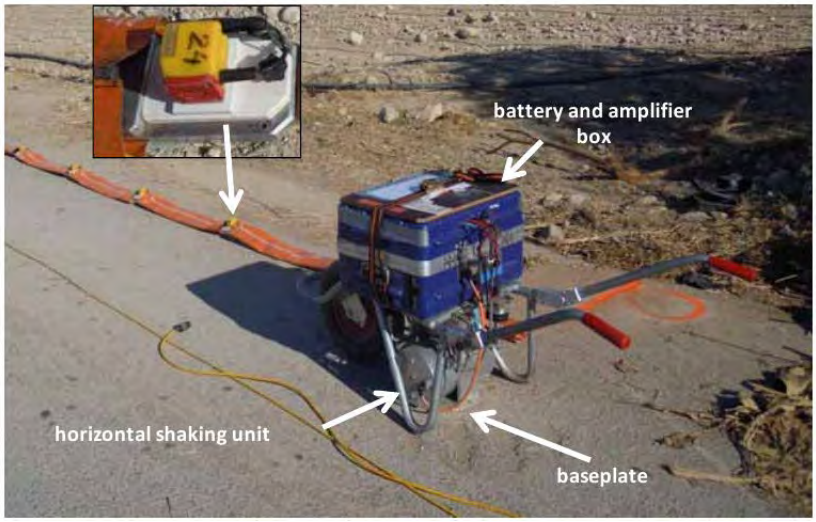

Figure 4.2 Wheel-barrow mounted vibratory shear wave seismic source system developed by LIAG. The electrodynamic driven shaker unit is mounted in the aluminium casing below the blue box, which contains the batteries and the amplifier unit. The analogue signal used for the shaking control is sent via the yellow wire from the operators place in the recording car. Small photo: horizontal geophone unit mounted on a skid system.

The system consists of an electrodynamic driven linear shaker unit mounted by airbag decoupling below the wheelbarrow frame (Polom et al., 2011) in a cubic casing (Figure 4.2). The typical shaking orientation is perpendicular to the direction of the wheelbarrow frame to generate a horizontally polarized (SH) shear wave. To use the vertically-polarized SV mode either the whole system or the shaking unit itself needs to be turned 90 degrees clockwise around the vertical axis (in terms of SEG convention). The driving control system consists of an amplifier, originally designed as a subwoofer driver for acoustic entertainment in cars. The main advantage of this control type is a more efficient conversion of electrical DC energy from the batteries into mechanical power than using a common AC amplifier unit e.g., used in stage acoustic technique.

Ground coupling is achieved by an aluminium plate below the casing, attached with small pyramid spikes to enhance friction on coarse surfaces. The maintaining weight and the initial system power is provided by a battery casing including the amplifier and a cascaded package of 12V batteries with 160Ah accumulator capacity in total. This enables the system to release more than 500 sweeps of 10 sec duration by one charge of the power pack, which is typically sufficient for more than ten hours of continuous high-production surveying. The resulting friction force below the baseplate is commonly enhanced by adding the source operator's weight on the top of the unit. The total weight is 110 kg (exclusive of the operator's weight), which can be handled by one person in the field and is small enough for transportation by car. The design and the generation of the source signals is achieved digitally using a software program running the common sweep (frequency modulated chirp signal) design formulas and special modification for signal forming additionally. After calculation, the digital source signals are subsequently stored into EPROM (Erasable Programmable Read-Only Memory) units, which are plugged into a digital-analogue converter unit to generate a highly reproducible analogous control voltage for the source system. The converter provides precise conversion timing, and generates the trigger signal to start the seismic recording instrument. Typically, this control unit is attached close to the recording instrument operation location to allow for fast modification of the source signal by the recording operator (exchange of EPROMs). Especially for S-wave operations, the analogue output signal can easily be reversed in polarity by operating a switch. This is convenient when using the so-called "plus-minus technique" similar to the opposite hammer blow on impulse S-wave source devices (e.g., Omnes, 1978; Dasios et al., 1999).

4.2.2 The receiver system

Instead of deploying planted, spike-attached horizontal geophones, as commonly used in seismic acquisition setups, a land streamer mounted geophone array, developed by LIAG (www.liag-hannover.de) and GEOSYM (www.geosym.de), was used (Figure 4.3). The ground coupling of the geophones is achieved only by the force of gravitation using a statically stable 3-point contact, which is attached by a plastic skid element. The whole geophone line including connectors and cables is mounted on a woven belt, which allows for easy and fast transportation and operation. During transport, the whole recording system remains connected, except that the power supply is disconnected for safety reasons (Figure 4.4).

Inazaki (2004) and Pugin et al. (2004, 2007) also demonstrated that land streamers are more efficiently operated and have an improved signal to noise ratio in urban environments compared to commonly used planted geophones. Inazaki (2004) reported that the use of such a system on paved surfaces leads to a suppression of Love surface waves, which usually strongly disturb SH polarised S-wave recordings. Foregoing tests at LIAG indicated that only a thin pavement at the surface is not sufficient to get satisfying results. Love wave suppression is efficient, if the top layer, where the direct SH polarized S-wave is propagating, is of higher velocity than the half space below. This is typically already the case for a rugged road construction, even if the surface is not paved with asphalt or concrete. In the case of concrete or asphalt pavement, the Love wave suppression is highly efficient.

Figure 4.3 Seismic land streamer receiver system (developed by LIAG and GEOSYM): a) during transportation including the dismounted source system; b) during release on site; c) during recording operation on Edgecumbe Fault slope site; d) during night operation in Whakatane. The geophone system was permanently connected to a GEODE seismic recording unit of 96 channels within the recording car at the front of the streamer, from where the recording operation was managed.

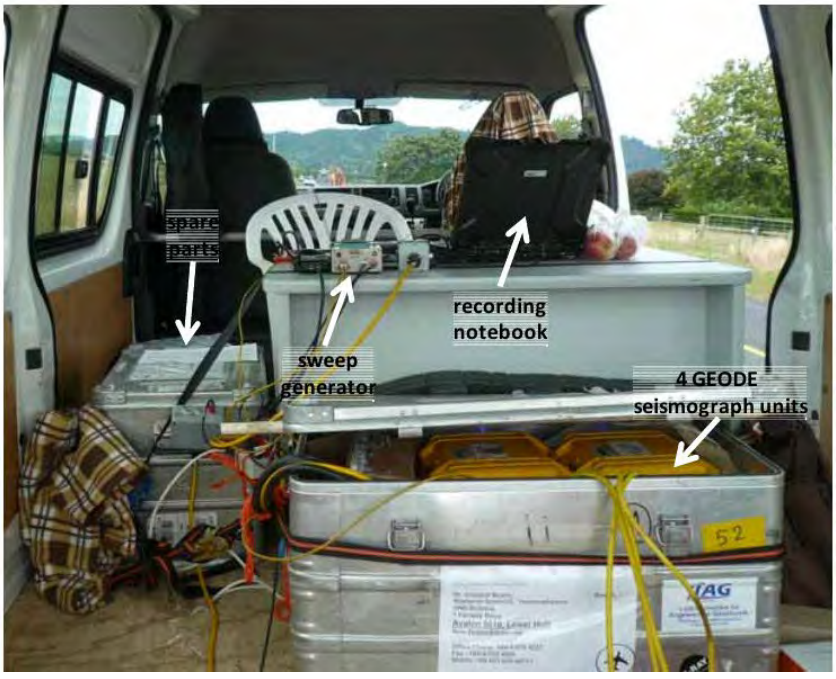

Figure 4.4 Recording equipment installation in the recording car and operators place. The yellow boxes within the aluminium box contain four GEODE seismograph digitizers connected to the recording notebook by an ethernet line. A pack of four 12 V batteries of 160 Ah in total are stored hidden below the table to enable sufficient power supply for several days. The sweep generator on top of the table creates the desired frequency modulated chirp signal (sweep) real time from a digital storage EPROM and initialises precisely the start of the data recording. The signal is sent parallel to the source and the recording system.

Figure 4.5 schematically shows the profiling operation used. In contrast to land streamer operations where the seismic source is connected ahead of the streamer and used both as a tracking and recording unit (e.g., Pugin et al., 2004, 2007, 2013), a source-receiver configuration scheme operating the source independently from the land streamer position was used. At a fixed streamer position, 15 source positions (4 m distance) were carried out from geophone sledges 24 to 72. Subsequently, the streamer was moved up 48 m by the recording car. This enables a variable split-spread configuration instead of an off-end configuration and an improved flexibility in the spread configuration, for example if the configuration needs to be changed at road crossings or elsewhere, to enable emergency access. Furthermore, this scheme reduces the total number of streamer move ups along a seismic profile, which strongly reduces the number of ground coupling problems of the streamer sledges. A similar configuration was used by Malehmir et al. (2015) during a land streamer operation in the city of Varberg, southwest Sweden.

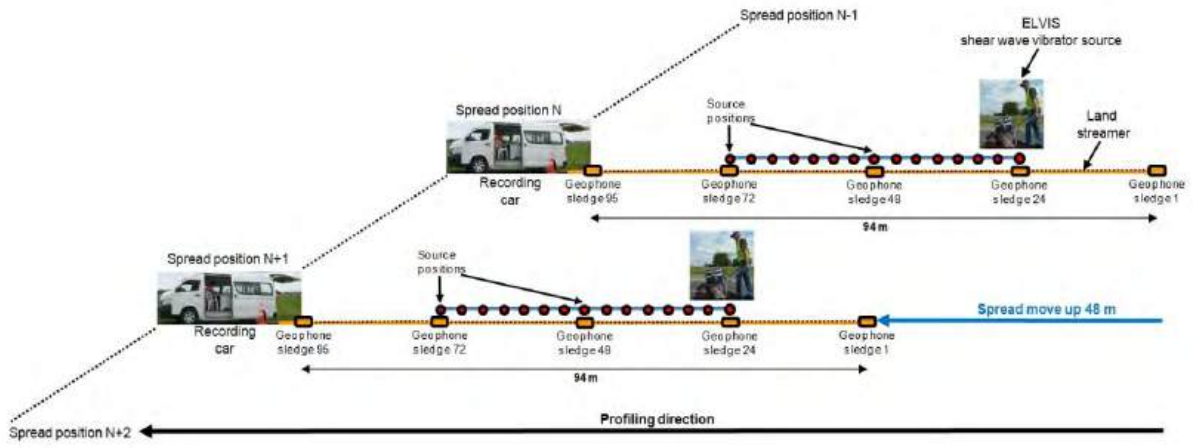

Figure 4.5 Schematic configuration of the data acquisition setup. Usually, 15 source positions of 4 m distances were carried out from geophone sledges 24 to 72. Then the land streamer was moved forward 48 m by the recording car, while the source stayed at its last position, meeting the geophone sledge 24 again if the move up was completed. After a short receiver coupling check to prevent bad traces, source operation from geophone sledges 24 to 72 started again. In difficult profiling locations, this scheme is flexible to be adapted to meet requirements imposed by the urban environment.

5.0 DATA PROCESSING

The data processing sequence applied to all survey data is illustrated by using profile 1 at the Edgecumbe site and profile 5 of the Whakatane site as examples. Beyond this, each profile required some specific processing slightly different from the others.

5.1 EDGECUMBE PROFILE 1

Figure 5.1 shows a single example record from profile 1, which crosses the Edgecumbe Fault nearly perpendicular to McCracken Road southwest of the village of Edgecumbe (see Figure 4.1 for profile location). Here, the surface trace of the Edgecumbe Fault is clearly visible in the terrain and expressed as a c. 4 m topographic step adjacent to the road. The trace was thoroughly documented after the earthquake in 1987 (Beanland et al., 1989).

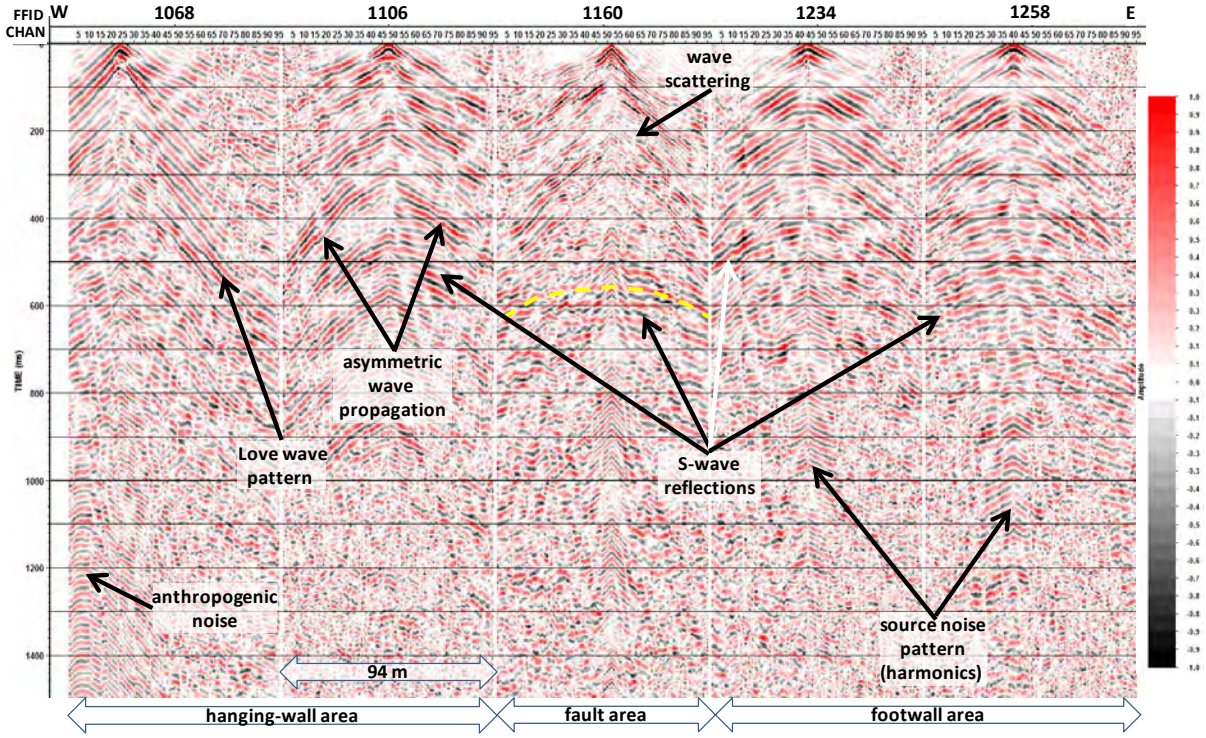

Figure 5.1 Examples of raw records from profile 1 across the Edgecumbe Fault (AGC 250 ms, Bandpass Filter 18-22-65-75 Hz) showing three zones of different wave propagation behaviour along the profile. In the western part (FFID 1068 and 1106) some Love waves of low velocity and an asymmetric propagation behaviour are dominant in the records, mostly covering the reflection signals. In the zone above the fault (FFID 1160), wave scattering is dominant in the upper part of the records, whereas clear reflections are visible below. In the eastern part of the profile the records consistently show a series of good quality reflections without disturbing wave parts. See Figure 4.1 for profile location.

The wave propagation behaviour is almost asymmetric with respect to the source position, which indicates an anisotropic subsurface structure. Furthermore, even though a uniform asphalt pavement of good quality is present at the surface, Love wave propagation is partly visible in the western part of the profile, indicating low velocity layers in the shallow subsurface. Tests to eliminate the Love wave portion in the raw records by applying a FK-filter led to unsatisfactory results, especially with respect to structural imaging near the fault area. The best result for the whole profile was achieved using a processing sequence without any suppression of undesirable parts of the wave field. The analysis of the velocity field required careful tests in a narrow velocity window required by the overall low velocity range of 50-250 m/s. The analysis was carried out using an interactive velocity analysis, combining several data imaging versions for a parallel analysis. An example from profile 1 is shown in Figure 5.2.

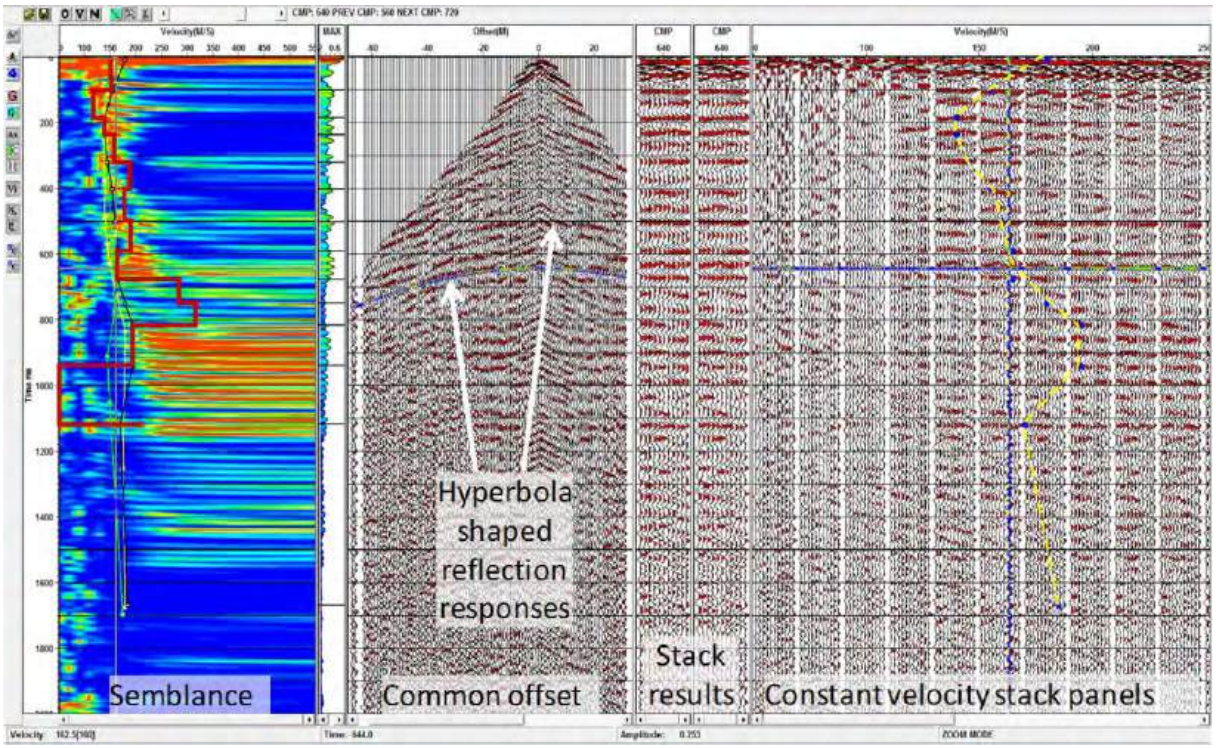

Figure 5.2 Screenshot example from Interactive Velocity Analysis at CMP 640 of profile 1 (Edgecumbe Fault) during the Brute processing. It mainly consists of a combination of three data imaging windows called Semblance, Common Offset Trace Gather (COG), and Constant Velocity Stack (CVS) panels. This analysis supports the verification of reflection responses indicated by the hyperbola curvature characteristics in the COG and the calculation of a best fitting NMO velocity-time-function (shown as yellow line in the CVS panel). Lines shown in the Semblance window image changes from previous CMP analysis location (green) to current CMP analysis location (black) and to next CMP analysis location (yellow). The red line shows the resulting interval velocity in time derived from the NMO velocity (black). Semblance window colours mark the resulting stacking energy (blue: low, red: high) depending on the velocity used. See Figure 4.1 for profile location.

The main data processing flow consisted of:

1. Vibroseis Correlation using the pilot sweep signal,
2. Vertical Stacking of records
3. Geometry Setup
4. Amplitude Scaling
5. Bandpass Filter
6. Top Muting
7. CMP-Sort
8. Interactive Velocity Analysis
9. CMP-Stacking
10. a) Frequency-Distance (FX) – Deconvolution
    b) Finite-Difference (FD) – Migration
11. Depth conversion of 10 a) and 10 b) using velocities derived in 8.

Iterations were applied between steps 8 and 11 to improve the processing results by reducing imaging artefacts and stabilizing the derived processing velocities for the final depth imaging. During the survey the geometry was defined using relative coordinates, since GPS data was not available till the end of the survey. A geometry update to absolute coordinates was carried out later during the final processing. Figure 5.3 shows the time domain processing result after Frequency-Distance (FX) -Deconvolution (step 10a).

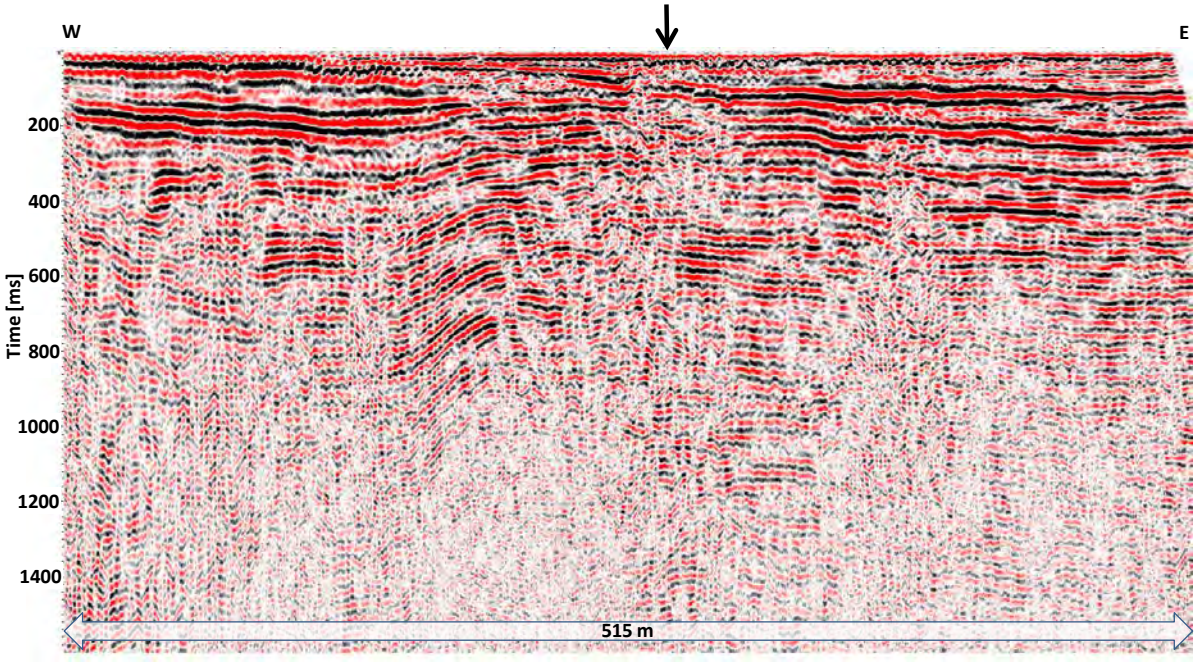

Figure 5.3 Resulting time section of profile 1 (Edgecumbe Fault) after application of FX-deconvolution used for lateral frequency alignment. The position of the surface scarp of the fault is indicated by the black arrow and the fault dips steeply (~70°) to the west (W). See Figure 4.1 for profile location.

Figure 5.4 shows the time domain processing result after FD-migration (step 10 b). The input of both processing steps was the output from step 9. The difference between both results is only apparent in details, especially for steeply dipping structures seen in Figure 5.3. This is a direct consequence of the low velocities and proves the migration process worked correctly.

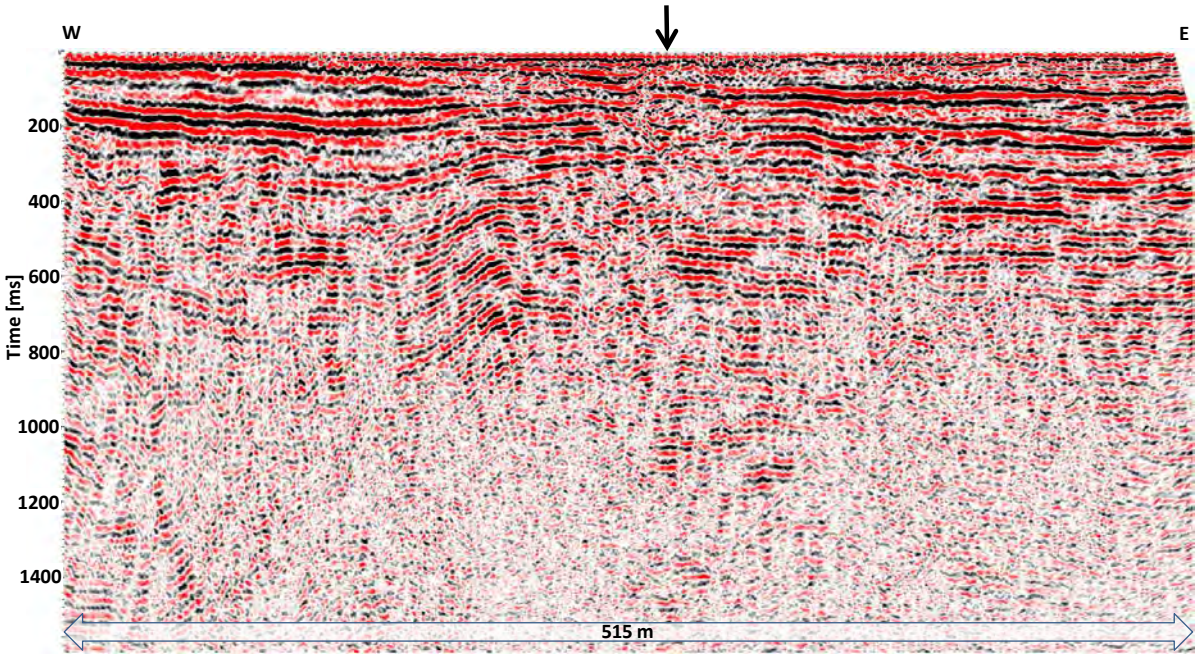

Figure 5.4 Resulting time section of profile 1 (Edgecumbe Fault) after FD-time migration to eliminate residual diffractions and to correct positions of dipping structures. Compared to Figure 5.3 the effect of this process is only small, which is mainly caused by the low velocities. The result of the process is also an indicator of quality to see whether the velocity field matches the data field. Topographic corrections are still not applied. See Figure 4.1 for profile location.

Subsequent to the time domain processing the time domain data was depth converted using a smoothed 2D velocity field (RMS velocities in time) derived from the results of several iterations of Interactive Velocity Analysis, which was also evaluated by the results of the FD-migration process and checked for lateral consistency. To consider the effects of topography, the datum level was set close to the maximum elevation of the profile track, in the case of profile 1 to 35 m a.s.l., to include all the data in the depth section. These static corrections were applied in the depth domain. The final depth section is shown in Figure 5.5 using a vertical-to-horizontal exaggeration of 2:1. An elevation profile is included at the top of the Figure. Figure 5.6 shows the same depth section result combined with colour coded interval velocities in depth derived from RMS velocities in time using the Dix equation (Dix, 1955).

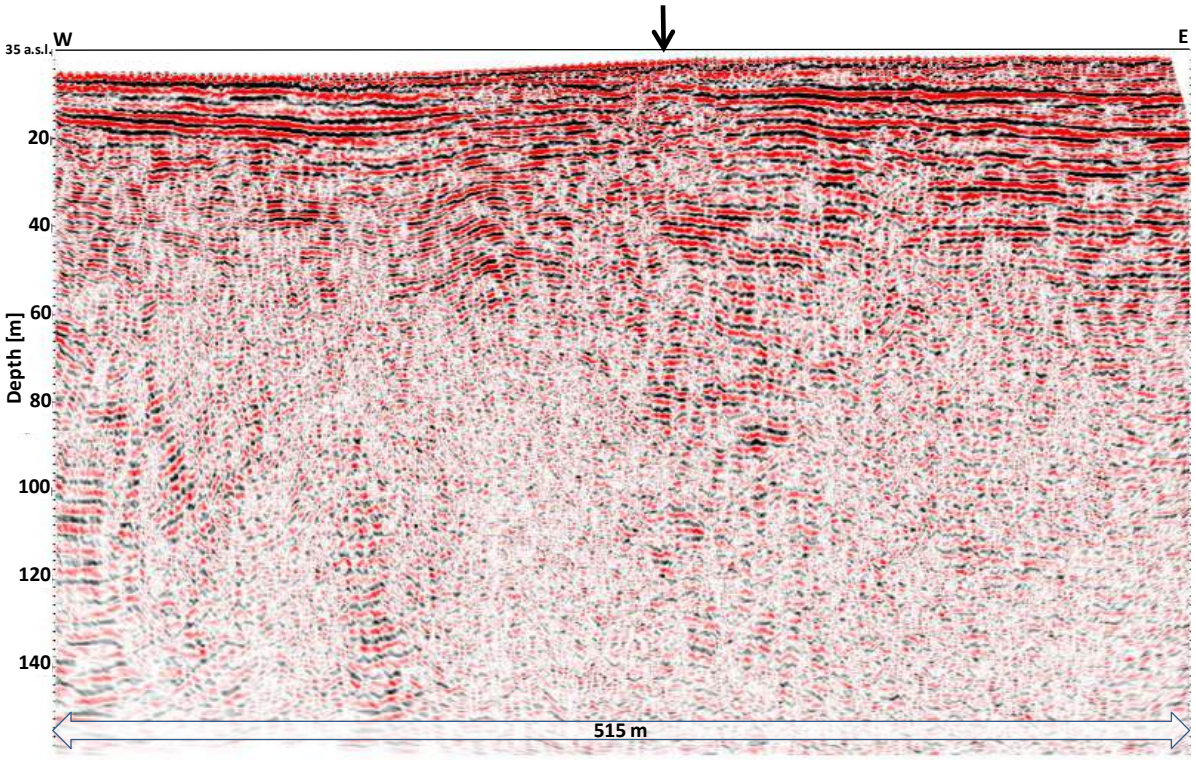

Figure 5.5 Resulting depth section of profile 1 (Edgecumbe Fault) in a horizontal-to-vertical scale of 1:2, based on velocities derived from the seismic data only. The depth range achieved is up to 100 m even though the velocity range was low with a mean of nearly 150 m/s. Topographic corrections are applied using 35 m a.s.l. reference datum. The upthrown (footwall) side of the fault (east of the arrow) shows a comparatively continuous and nearly horizontal reflector pattern, while the downthrown side (hanging wall) shows a disrupted pattern and increasing dips in depth to the west, forming a basin structure. Reflectors on the hanging wall adapt to the shape if the basin (subsidence on this side of fault) and laps show slight tilting to the east, away from the fault, a feature typical of a normal component on the fault. At depth, the fault trace is not clearly imaged as a specific reflector, it is indicated by a set of reflector offsets (ruptures), reflector disruption (not clearly delineated) and ductile deformation structures (folding). See Figure 4.1 for profile location.

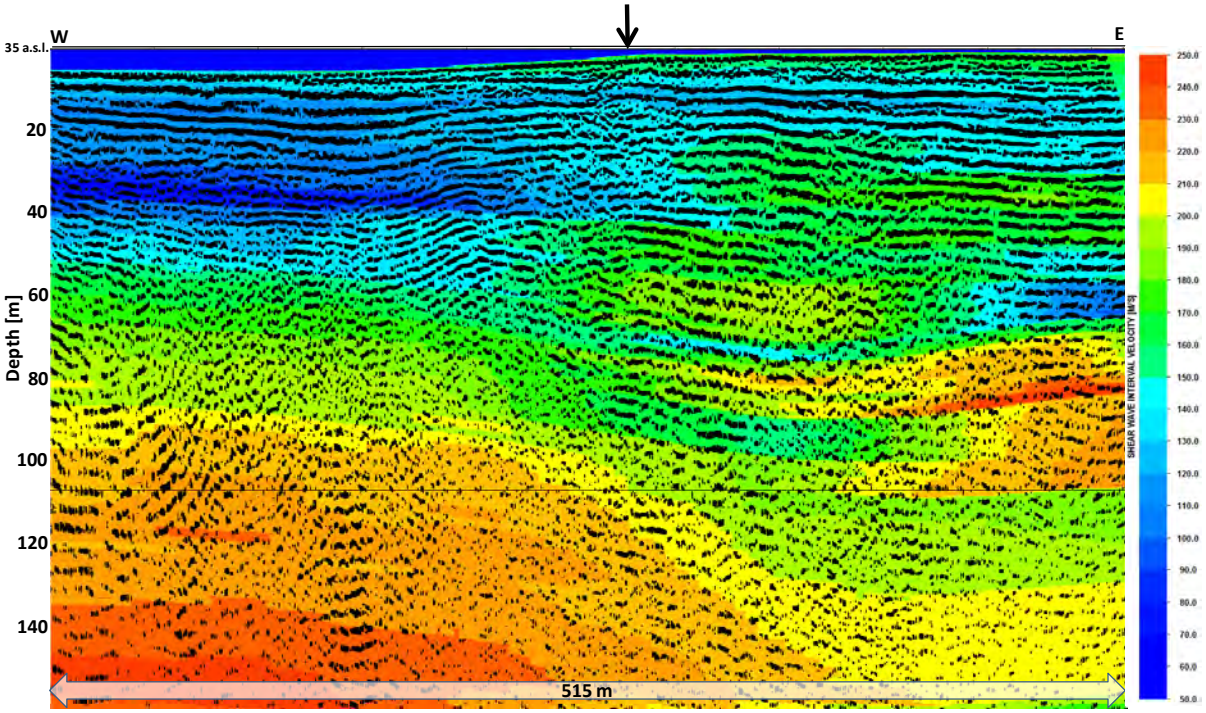

Figure 5.6 Resulting depth section of profile 1 (Edgecumbe Fault) colour coded by shear wave interval velocities in depth derived from the seismic data (horizontal-to-vertical scale of 1:2). Due to the limited offset range of the survey setup, velocities below 80 m may be erroneous. The blue zone on top left is caused by topographic corrections applied (reference datum 35 m a.s.l.). Combining the structure and velocity information supports the fault trace identification at depth, which is obviously not a straight line, more characterized by stacked zones of disturbed reflector patterns at depth. The reflector pattern 10 m below the arrow mark shows a fault offset of 2-3 m. See Figure 4.1 for profile location. For an interpretation of these data refer to Figure 6.1.

5.2 WHAKATANE PROFILE 5

Figure 5.7 shows single record examples of profile 5, which was acquired along Stewart Street in Whakatane (see Figure 4.1 for profile location).

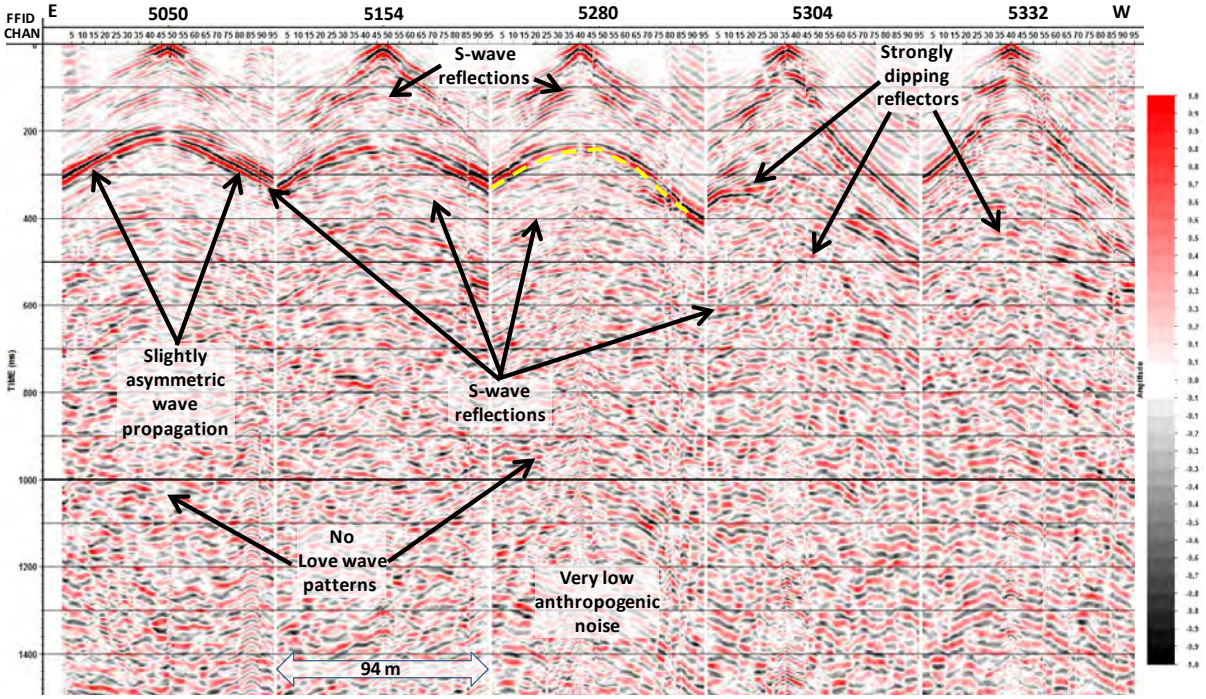

Figure 5.7 Example of raw records for profile 5 (AGC 250 ms, Bandpass Filter 18-22-65-75 Hz) along Stewart Street. In the eastern part (FFID 5050, 5154, and 5028) a strong reflector with its top near 200 ms is visible which is seen on all profiles and used as a marker horizon for the Whakatane area. In the western part (FFID 5305 and 5332) this reflector shows a strong dip towards West. Love waves do not affect the records, indicating absence of significant low velocity channels in the subsurface. Due to the night time survey effects of anthropogenic noise and wind noise are very low in general. See Figure 4.1 for profile location.

The three records FFID 5050, 5154, and 5028 at the left show a significant marker reflection with top near 200 ms, which is present in nearly all profiles in the Whakatane area. Already in the raw records, this reflection shows details of the subsurface structure, allowing excellent quality control during data recording. Over the first 550 m of the 671 m long profile this marker reflection was quite stable, but changed to a strongly west-dipping structure beyond 550 m (e.g., FFID 5305 and 5332). The seismic reflection characteristics also change above the marker reflection in these two records, indicating lower propagation velocities. This is the first strong subsurface anomaly found during the Whakatane survey. The clear signature of the marker reflector enabled a high-quality velocity determination, shown by example in Figure 5.8.

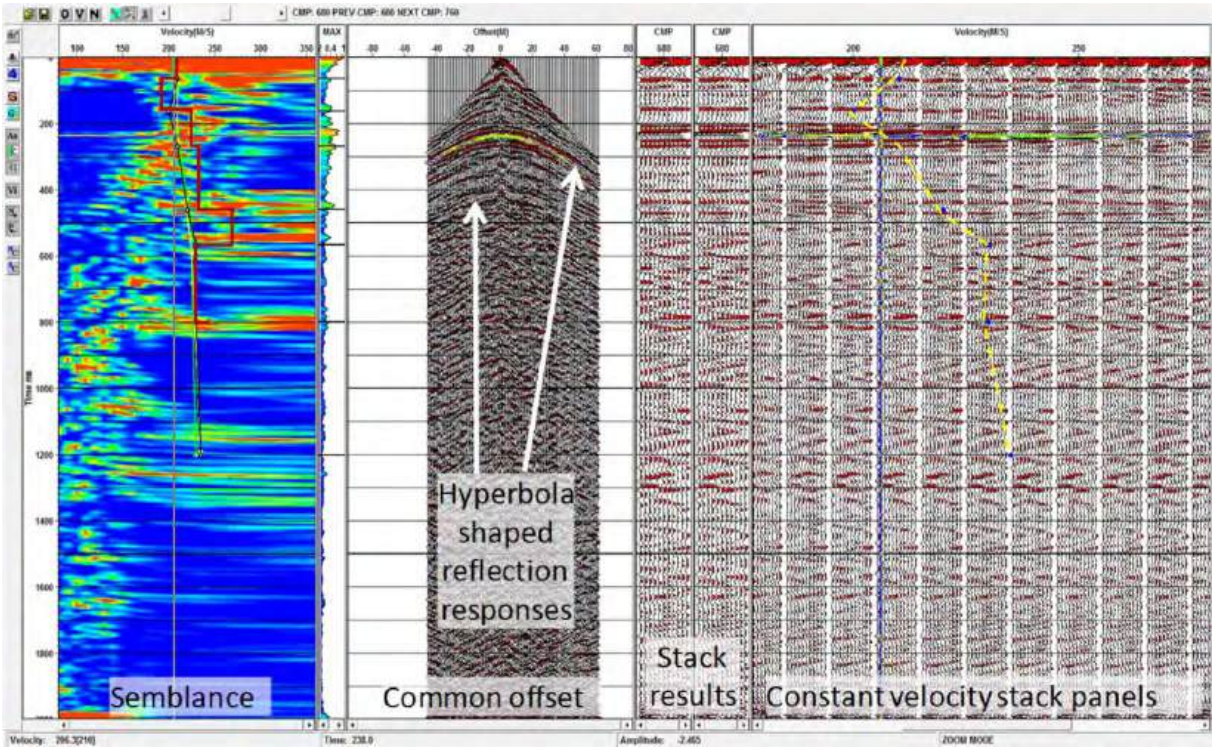

Figure 5.8 Screen shot example from Interactive Velocity Analysis at CMP 680 of profile 5 in Whakatane township. For the marker reflector a mean velocity of nearly 200 m/s can be determined with good precision, providing an estimated depth of nearly 20 m. surrounding wavelet signatures indicate a vertical resolution of less than one metre. Below 20 m the precision of the velocity determination and the resolution decreases due to lower reflection strengths and, below 600 ms, due to the restricted offset range of the survey setup. See Figure 4.1 for profile location.

Figure 5.9 shows the time domain data processing result after Frequency-Distance (FX) - Deconvolution (step 10 a). Figure 5.10 shows the time domain data processing result after FD-migration (step 10 b). The final depth section is shown in Figure 5.11 with a vertical exaggeration of 2:1. Again, an elevation profile is given in the top part of the figure. The final elevation datum was set to 33 m a.s.l. and finally, Figure 5.12 shows the same depth section result combined with colour coded interval velocities in depth derived from RMS velocities in time using the Dix equation (Dix, 1955).

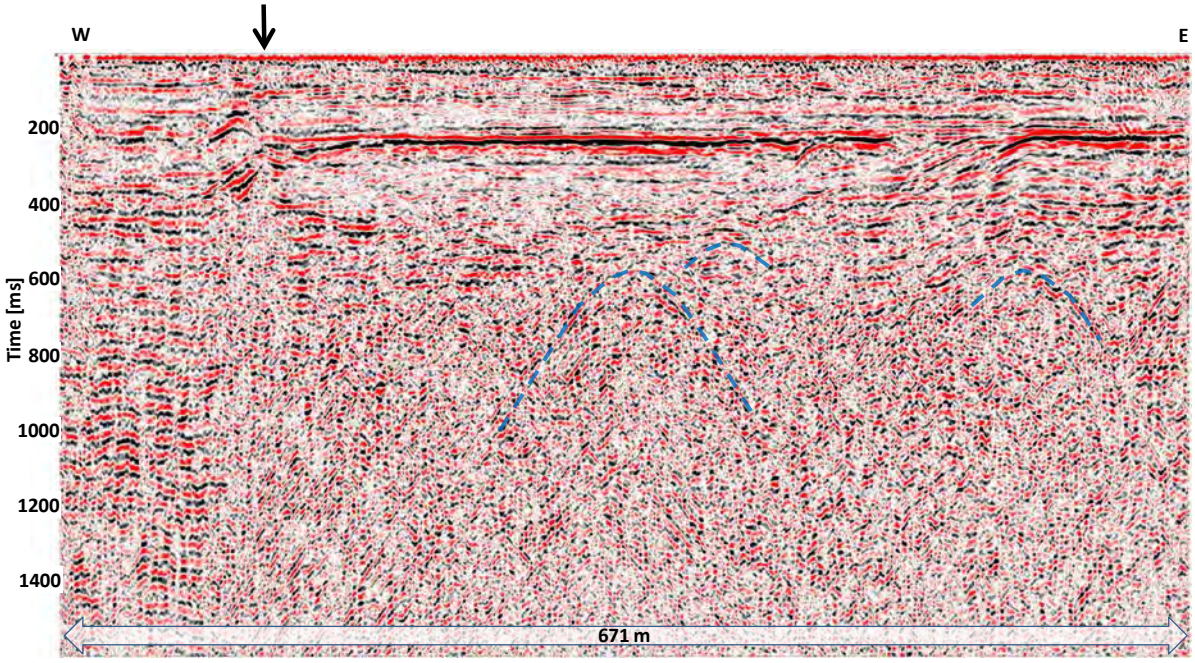

Figure 5.9 Resulting time section of profile 5 in Whakatane township after application of FX-deconvolution used for lateral frequency alignment. The black arrow on top of the section marks the position of the anomaly found for the marker reflector and in the surrounding structures. It indicates the location of the Whakatane Fault as interpreted from the near-surface disruption of layers recorded in the land streamer data. Below 500 ms weak diffraction patterns (dashed blue lines) are visible, probably caused by small discontinuities of less than a wavelength in the subsurface. See Figure 4.1 for profile location.

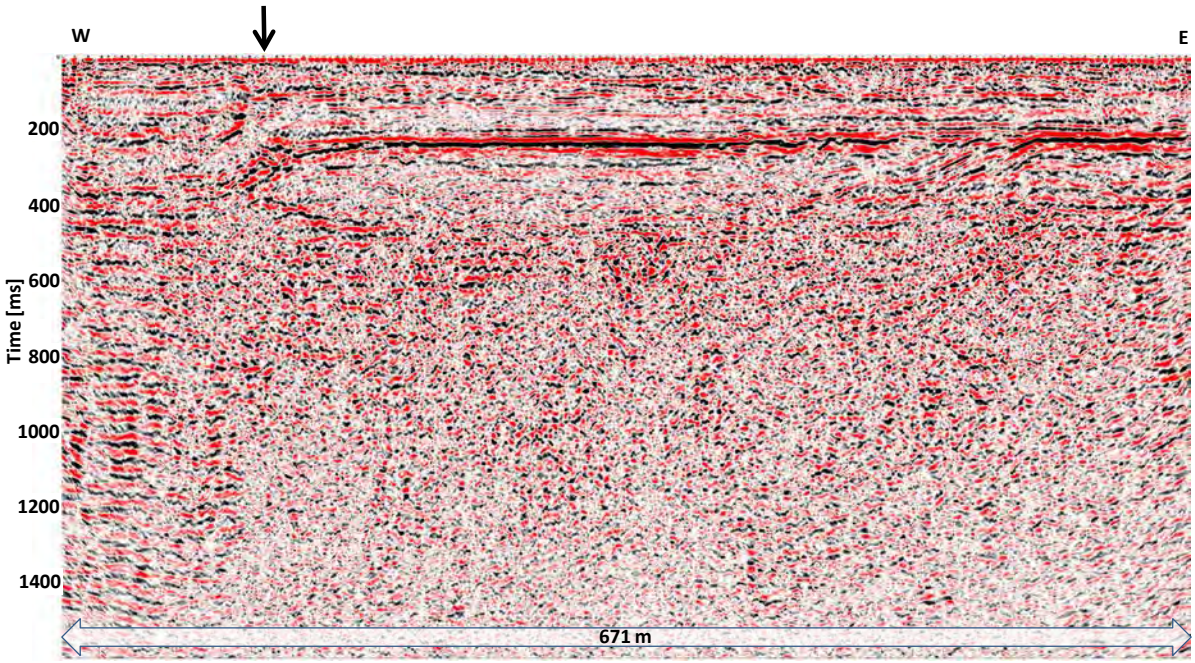

Figure 5.10 Resulting time section of the FD-time migration process along profile 5 in Whakatane township. FD-time migration eliminates residual diffractions and corrects the position of dipping structures. See Figure 4.1 for profile location.

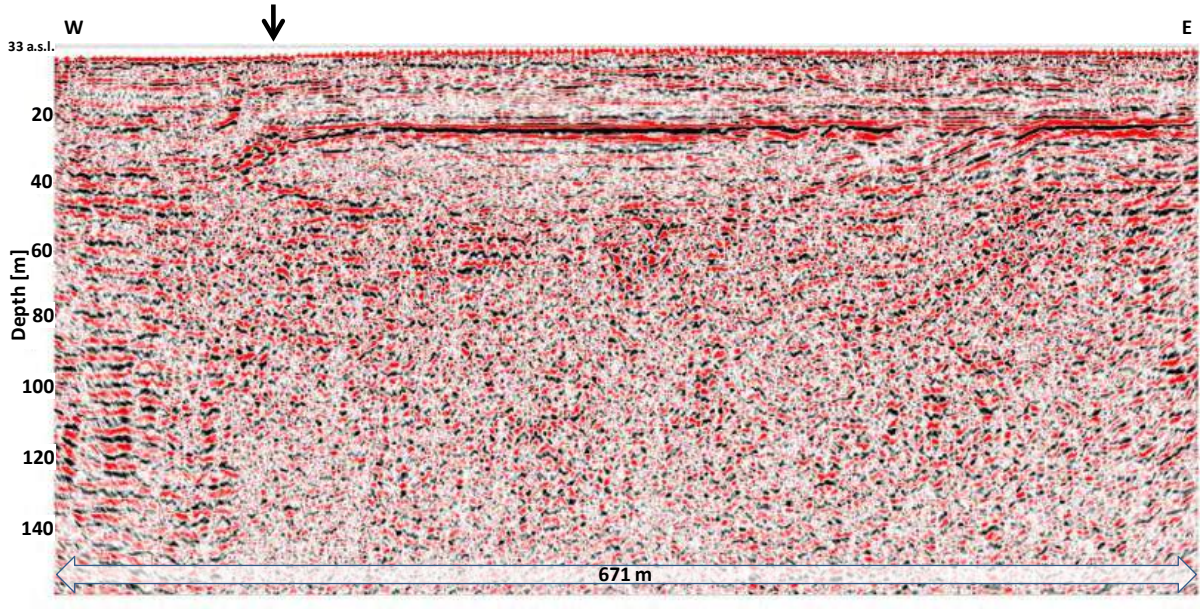

Figure 5.11 Depth section of profile 5 in Whakatane township based on velocities derived from the seismic data only and with a horizontal-to-vertical scale of 1:2. The depth range of seismic reflectivity achieved is up to 100 m, the mean velocity is nearly 200 m/s. Topographic corrections are applied using 33 a.s.l. reference datum. See Figure 4.1 for profile location.

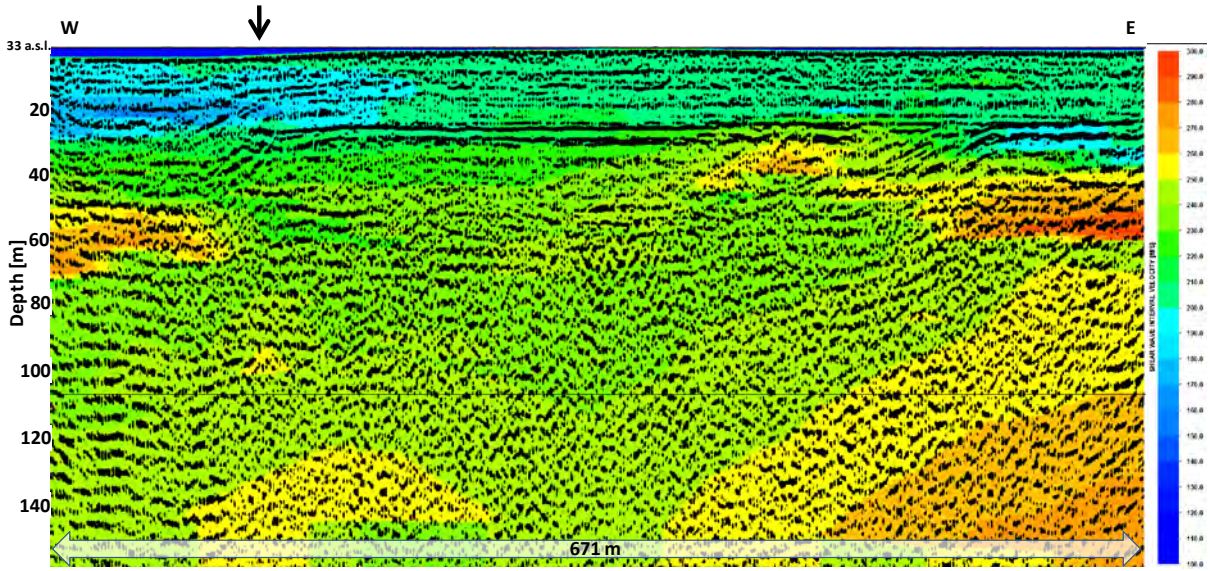

Figure 5.12 Depth section of profile 5 in Whakatane township colour coded by shear wave interval velocities in depth derived from the seismic data (horizontal-to-vertical scale of 1:2). Due to the limited offset range of the survey setup, velocities below 80 m may be erroneous. The blue zone on top left is caused by topographic corrections applied (reference datum 33 m a.s.l.). See Figure 4.1 for profile location.

This page is intentionally left blank.

6.0 INTERPRETATION OF RESULTS

Our final processed profiles show a number of characteristics of the Edgecumbe survey that clearly indicate the position of the fault beneath its surface trace in unconsolidated sediments. In this section we will discuss the locations, geometries and displacement of active faulting in Whakatane and compare these results with the Edgecumbe Fault profiles. Note that this report only presents a preliminary geological interpretation of potential active faulting from the seismic lines acquired; a full interpretation is beyond the scope of this study.

6.1 EDGECUMBE

The expression of the fault in the near surface in high-resolution shear wave seismic images (up to just about 1 m below ground level) is not well documented in the literature simply due to the limited collection of this kind of data. Kurahashi and Inazaki (2007) carried out an investigation of a buried active fault in Japan using a shear wave vibrator source. For this reason we are using the seismic images crossing the known Edgecumbe Fault trace as a reference for interpretation of those from Whakatane. We were expecting the seismic profiles to replicate structures such as those documented in excavations of active fault traces including the Edgecumbe Fault (e.g., disrupted subhorizontal sedimentary layers, faulting, folding and fissuring: Beanland et al., 1989) or those of the Whakatane Fault (Mouslopoulou et al., 2009). It is important to note that the Whakatane Fault has a strike-slip component of slip as well as a normal component, while the Edgecumbe is almost purely normal. Imaging deformation due to a strike-slip motion could be achieved but would require a different layout of seismic profiles. However, we expect to be able to compare seismic profiles of the Whakatane and Edgecumbe faults on the basis of their common normal component of motion. Faulting expression in landstreamer seismic lines should also be similar to other seismic surveys in the region (e.g., offshore high-resolution seismics; Taylor et al., 2004), although those surveys were undertaken using different equipment and for deeper penetration.

We repeat Figure 5.6 here as Figure 6.1 for convenience to the reader and to illustrate the following discussion. The Edgecumbe Fault scarp mainly resulted from the 1987 rupture (Beanland et al., 1989) and is preserved as a step in the topography (located by a black arrow in Figure 6.1). A subdued topographic scarp (< 1.5 m in height) existed at this location prior to the 1987 Edgecumbe Earthquake, and based on trenching, formed during one or two prehistoric surface ruptures (Beanland et al., 1989).

Our seismic images consistently show continuous seismic reflectors on the upthrown and downthrown sides of the fault, separated by an area of disrupted reflectors close to the location of the fault scarp (black arrow in Figure 6.1)). It is difficult to identify a single fault plane in the seismic image as the fault seems to be expressed as a transitional zone. This is also expressed by the clear change in seismic velocities across the fault zone ranging from about 130 m/s on the upthrown side to about 80 m/s and less on the down thrown side in the topmost 30 m. The distributed sub-surface deformation is not surprising as the surface fault rupture associated with the 1987 earthquake shows a band on deformation with several fault planes in the near surface, including folded sediments (monoclinal folding) and pervasive fissuring (cracking). Our seismic images show eastward dipping bedding to the east of the fault, basin development to the west of the fault and drag folding around the fault in the uppermost 15 m (see Figure 6.1) and also compare with Figure 5.6).

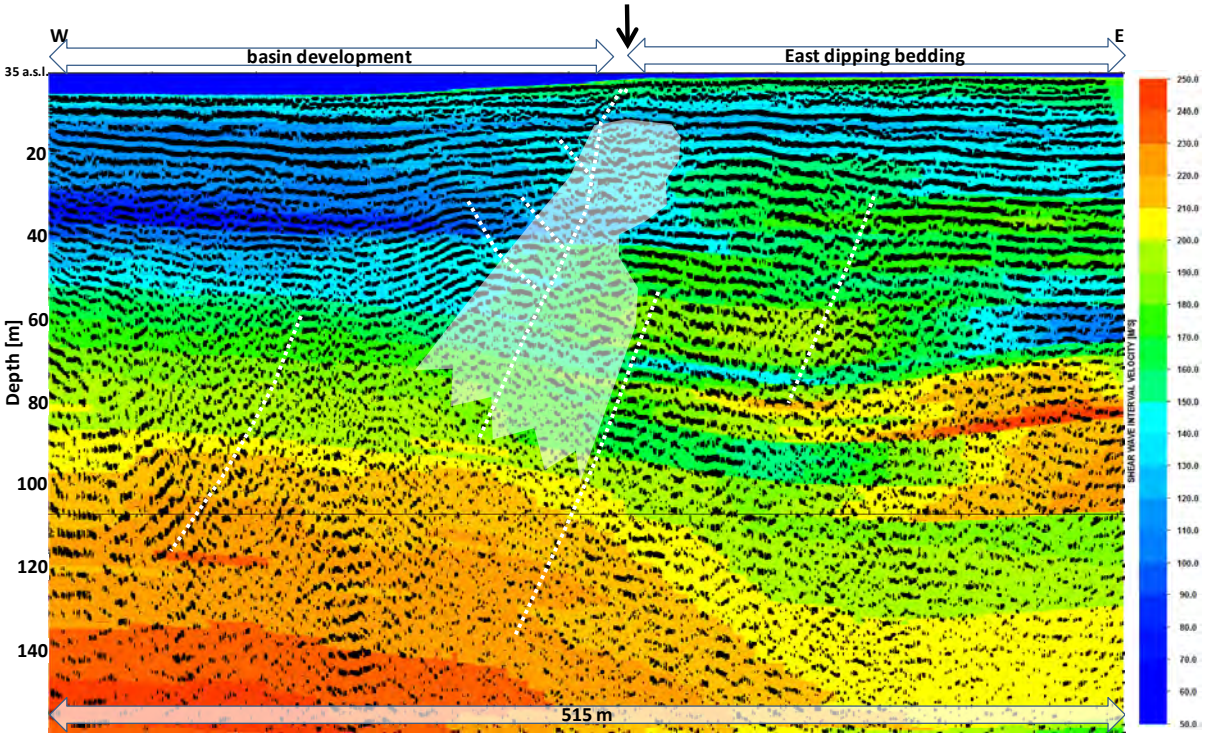

Figure 6.1 Edgecumbe profile 1 along McCracken Rd. showing seismic reflections and the shear wave interval velocity structure. White dotted lines indicate fault traces interpreted to produce layer disruptions; the white shaded zone indicates an area around the 1987 Edgecumbe central fault trace where reflector disruptions and signal scattering are highest. Due to the limited aperture of the land streamer receiver system, velocities below 80 m may be erroneous. See Figure 4.1 for profile location.

The other profiles imaging the Edgecumbe Fault show similar lateral structural and velocity changes but are not as clear as in the McCracken Road profile. The surface conditions along those farm tracks compromised data acquisition and data has more noise. Overall the survey across the Edgecumbe Fault trace was useful as a calibration experiment and provides an example of the structural near-surface expression of a demonstrably active fault displacing the unconsolidated materials typical of the Rangitikei Plains.

6.2 WHAKATANE

Fault scarps of the Whakatane Fault have been mapped south of Whakatane city (see Figure 2.1) but the exact location across the city has only been inferred (Leonard et al., 2010; Langridge et al., 2016). In some of the land streamer profiles across the township of Whakatane we observe similar disrupted reflectors to those of the Edgecumbe Fault. Figure 5.11 and Figure 5.12 show profile 5 acquired along Stewart Street. On this and all other profiles through Whakatane (e.g., Profile 4, Figure 6.2) we observe a marker horizon that runs mostly uninterrupted at about 20 m depth in the eastern part of the profiles. This horizon is correlated with the sedimentary sequence observed in a recent study of subsurface materials of the Central Business District of Whakatane (Begg et al., 2015).

Figure 6.3 shows a view from the north of a 3D geological model of Whakatane (Begg et al., 2015). The study produced a 3D geological model which provides independent data on which to correlate the prominent marker in our seismic profiles. Begg et al. (2015) suggest that the lower yellow geological horizon represents the boundary between dense Late Holocene non-marine silt and overlying Early Holocene marine sediments, dominated by sand. The depth of the boundary is c. 15 to 20 m below sea level.

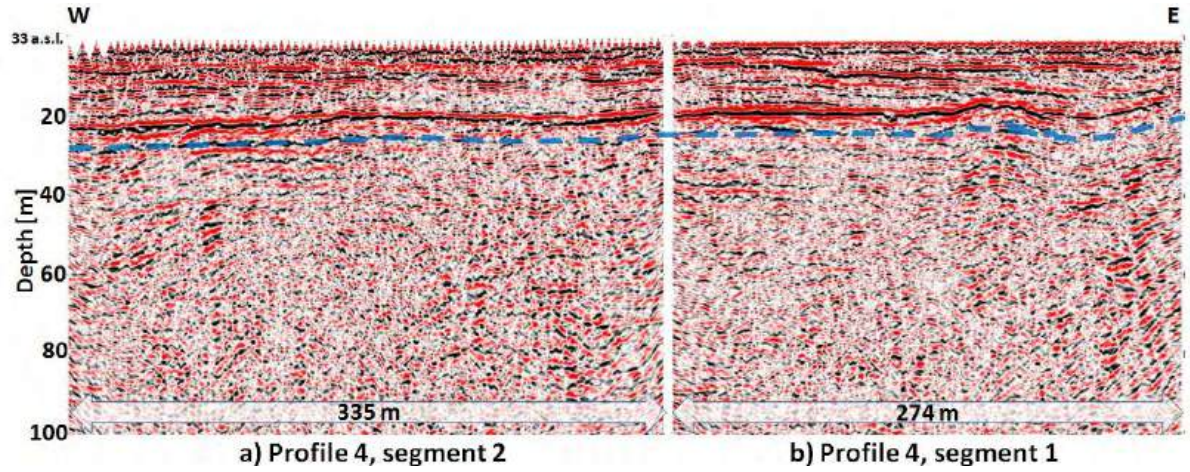

Figure 6.2 Depth sections of profile 4 with a horizontal-to-vertical scale of 1:2 (each). The profile was acquired in two segments (2, west, 1 east) along Goulstone Rd. The profile clearly exhibits a marker horizon (blue dashed line traces the horizon slightly deeper to avoid concealing it), which correlates well with findings in Begg et al. (2015)(see Figure 6.3). Figure 4.1 provides profile location.

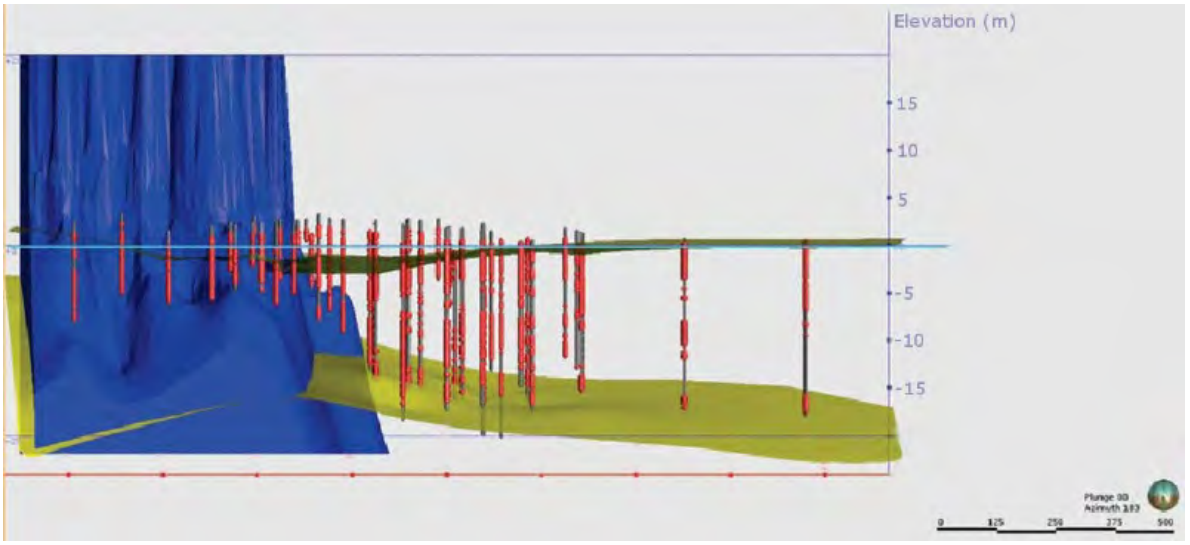

Figure 6.3 Whakatane CBD showing locations of Cone Penetration Testing (CPT) and boreholes (Begg et al., 2015). The study produced a 3D geological model which provides independent data on which to correlate the prominent marker in our seismic profiles. The lower yellow interface marks a horizon between early Holocene marine and underlying non-marine materials. The marine deposits above the horizon are characteristically dense sands and the underlying materials are dense non-marine silts. The boundary is assumed to produce the reflections associated with the continuous marker horizon observed in our seismic sections.

The seismic marker horizon observed around 20 m depth in our seismic lines may represent this boundary. Such a sedimentary boundary is expected to produce a strong impedance change and therefore a strong reflection. In addition, the horizon is continuous through the 3D geological model as it is on the seismic images. On profile 5 (Figure 5.11) the marker horizon is interrupted at point 550 m (counting from the east; see arrows in Figure 5.11) and the reflectivity structure changes significantly. This change is accompanied by a change in shear wave velocity structure in the upper 20 m (Figure 5.12). Similar seismic attributes were observed at the Edgecumbe Fault, and we infer that they mark the location of the Whakatane Fault on profile 5.

As at McCracken Road where the Edgecumbe Fault scarp is unequivocally visible at the surface, on profile 5 (Stewart Street), a change in topography coincides with the velocity and structural changes in the subsurface. Figure 6.4a is a photograph at the position of profile metre 550 on profile 5. The step in the terrain, dropping to the west, is less obvious than at the Edgecumbe Fault, but could represent a fault scarp (see further discussion below).

Similar changes to those seen in the seismic structural and velocity images in profile 5 are present on all profiles acquired in the town (see Figure 4.1 for profile locations). Figure 6.4b shows the combined velocity and structural seismic image again with an interpretation of the location of the fault indicated by the dashed white line. The step in surface topography is not observed along all profiles, but it is also present at the west end of profile 7 (see Figure 6.5) along James Street. Profile 7 is an eastward extension to profile 6, acquired after the first two-thirds of profile 6 were carried out.

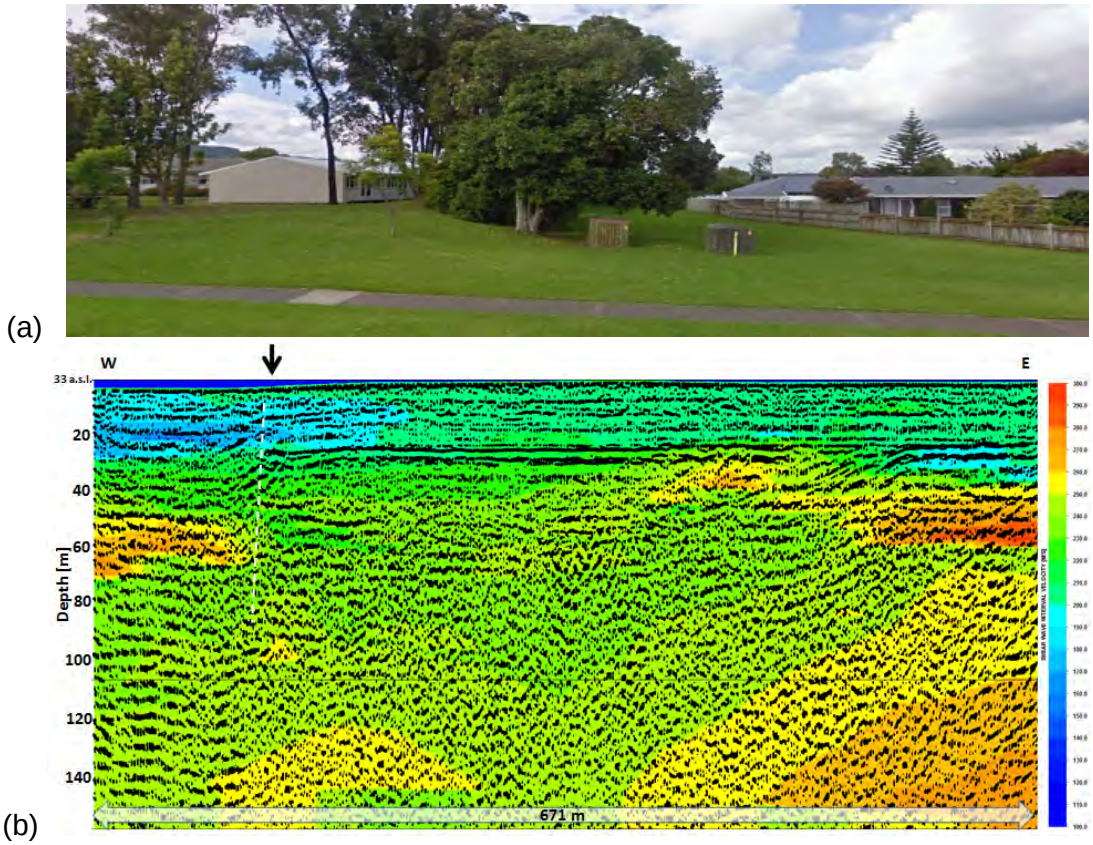

Figure 6.4 a) View to the south on Stewart Street at profile metre 550, Profile 5. The step in the terrain is obvious and is also observed further north on James Street (Profile 7) and Victoria Avenue – for further discussion see text. b) Same as Figure 5.12 but with an interpretation of the location of the fault (white dashed line) based on changes in reflectivity patterns, seismic velocity structure and discontinuation of the marker horizon.

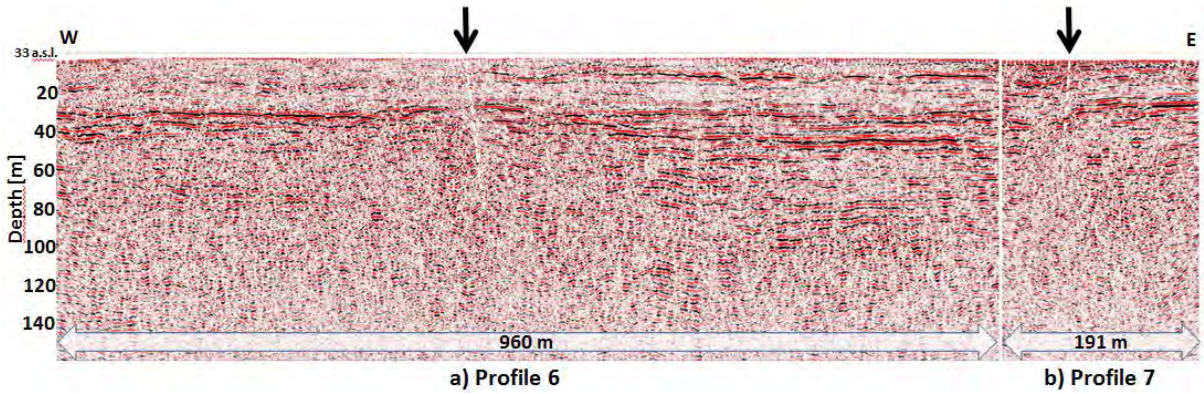

Figure 6.5 Combined seismic image (FD migrated depth sections) of profile 6 and 7 along James Street. The right side arrow (eastern part of the profile) indicates the approximate position of the step in the terrain observed at the surface in James Street. The arrow on the left (Western part of the profile) shows additional indication of faulting mainly based on a vertically staggered diffraction structure in the non migrated time section. The dashed white lines show interpretations of faulting on these profiles. Further descriptions in text. See Figure 4.1 for profile locations.

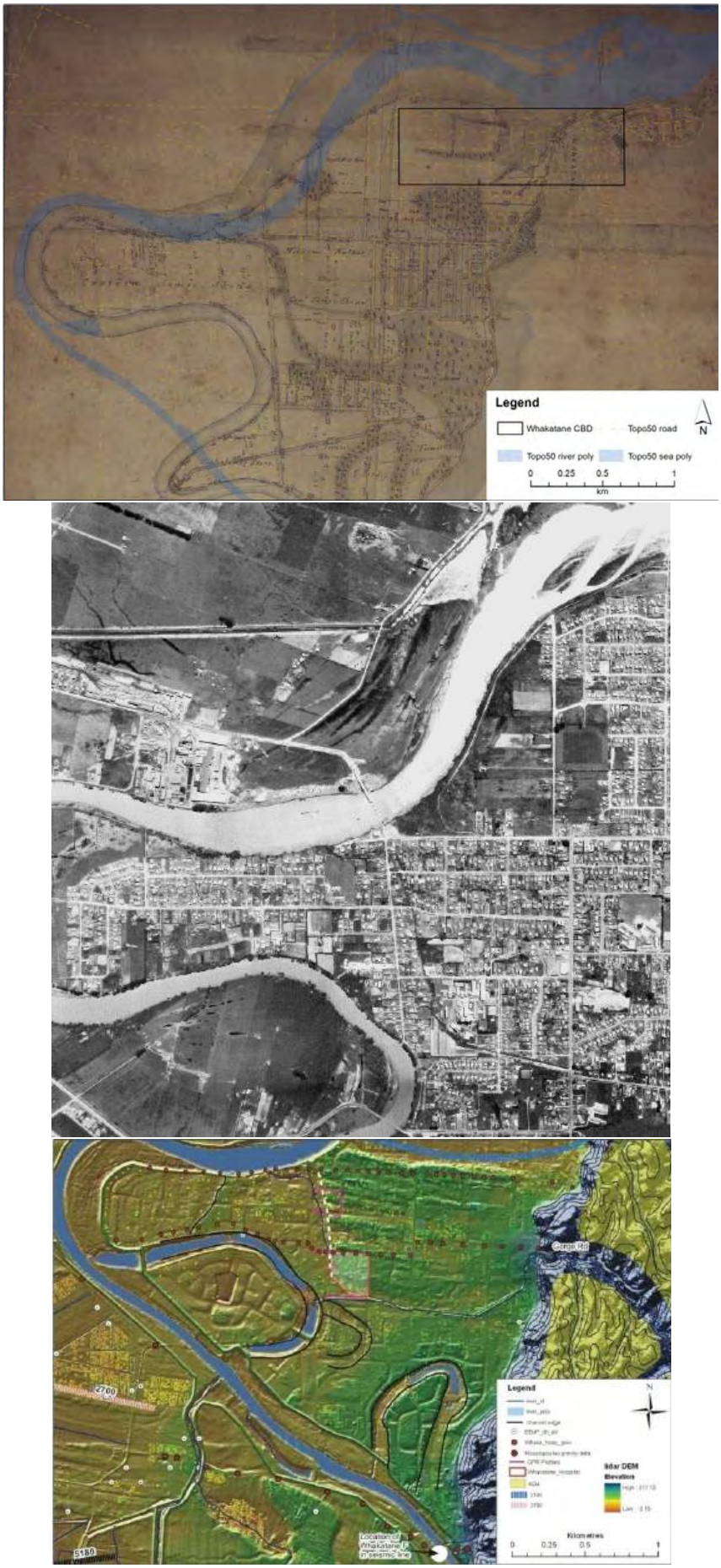

Figure 6.6 a) Whakatane District Council archival map dated 1867 (Begg et al., 2015) showing a swamp and stream system following the surface features discussed here. b) Aerial photograph from 1988 (Lands and Survey Department, Wellington, New Zealand, photo number 3331/47). c) The LIDAR image of the area also shows this feature (white dashed line).

Profile 7 was acquired to assess whether the step in the terrain was associated with similar subsurface structural changes as seen on the Stewart Street profile (Profile 5). It should be noted that this surface scarp has been modified at its northern and southern ends by an engineered underground stream channel entrance and exit.

Figure 6.6a shows a map dated 1867 (Begg et al., 2015) which documents the surface features to represent a vegetated (swampy) stream bed. On an aerial photograph taken in 1988 and the most recent digital terrain model derived from LIDAR data (Figure 6.6b and c) this surface feature is clearly expressed. It is possible that the topographic step spatially coincident with disrupted seismic reflectors is a fault scarp.

Further to the south, profiles at Bridge Street and Olympic Drive and Arawa Road (profiles 8, 9 and 10, respectively) reveal similar subsurface structures. The profiles at Olympic Drive and Bridge Street (profiles 8 and 9) both show a strong reflector at ~ 20 to 25 m depth that we correlate with the top Early Holocene marker horizon (Figure 6.7 and Figure 6.8). This horizon has several interruptions (vertical offsets; arrows on profiles) although the only significant change in deeper seismic reflection patterns is near the west of the Bridge Street profile (see oval in Figure 6.7; Profile 8). A similar change in reflection pattern was observed in profiles 6 and 7 (Stewart Street and James Street) and in the Edgecumbe Fault profiles. If these steps are indeed fault related, it is possible that the location of the main fault strand is associated with a significant change in the deep seismic pattern while other steps correspond to secondary fault strands (strands with minor deformation).

Figure 6.9a shows the depth migrated section along Arawa Road (profile 10). The seismic reflectivity pattern is more complex here (than the other Whakatane profiles), with several interruptions of the marker horizon (arrowed in Figure 6.9a). The seismic profile along Arawa Road is closer to the last known location of the Whakatane Fault in the south. The stacked section in Figure 6.9b shows the data prior to migration. This stage of seismic imaging still shows energy scattered from the edges of interrupted and truncated horizons as diffractions. The migration process removes those by mapping them onto the edges or truncations giving a proper image of the structure. Diffractions are often used as fault indicators. The same observation was made in the profile acquired along James St (profile 6).

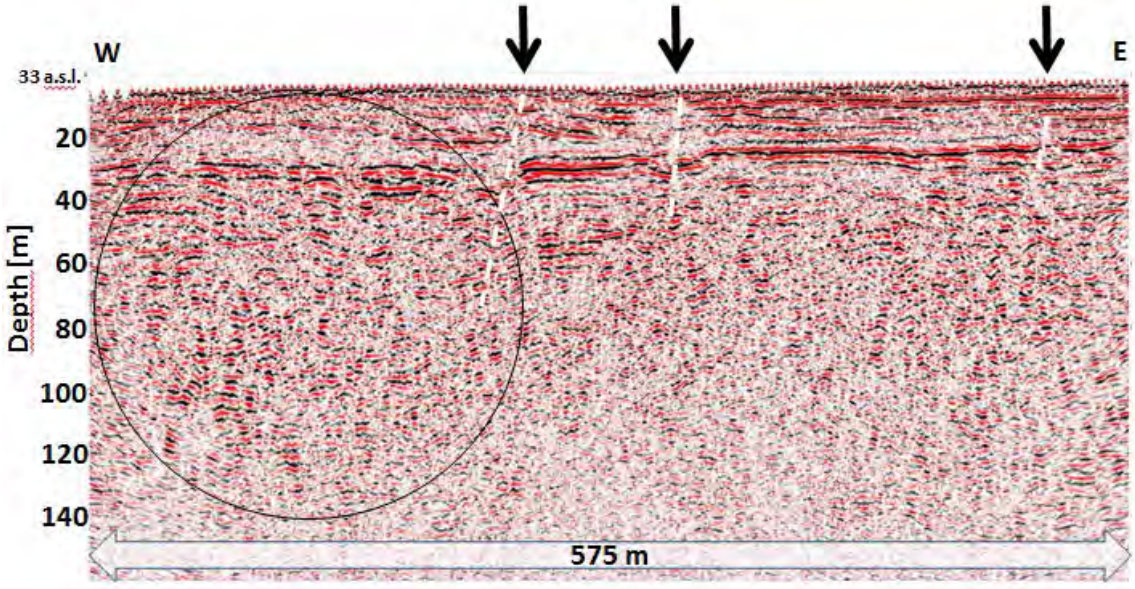

Figure 6.7 Depth converted migrated section of profile 8 along Bridge Street, Whakatane. Note the continuous reflection of the marker horizon nearly 20 m depth below surface in the east that is interrupted at least twice (arrows). It becomes less continuous to the West (circled area) where also dipping structures and increased scattering occur below the marker horizon. The dashed white lines are interpretations of faulting on this profile. See Figure 4.1 or profile location.

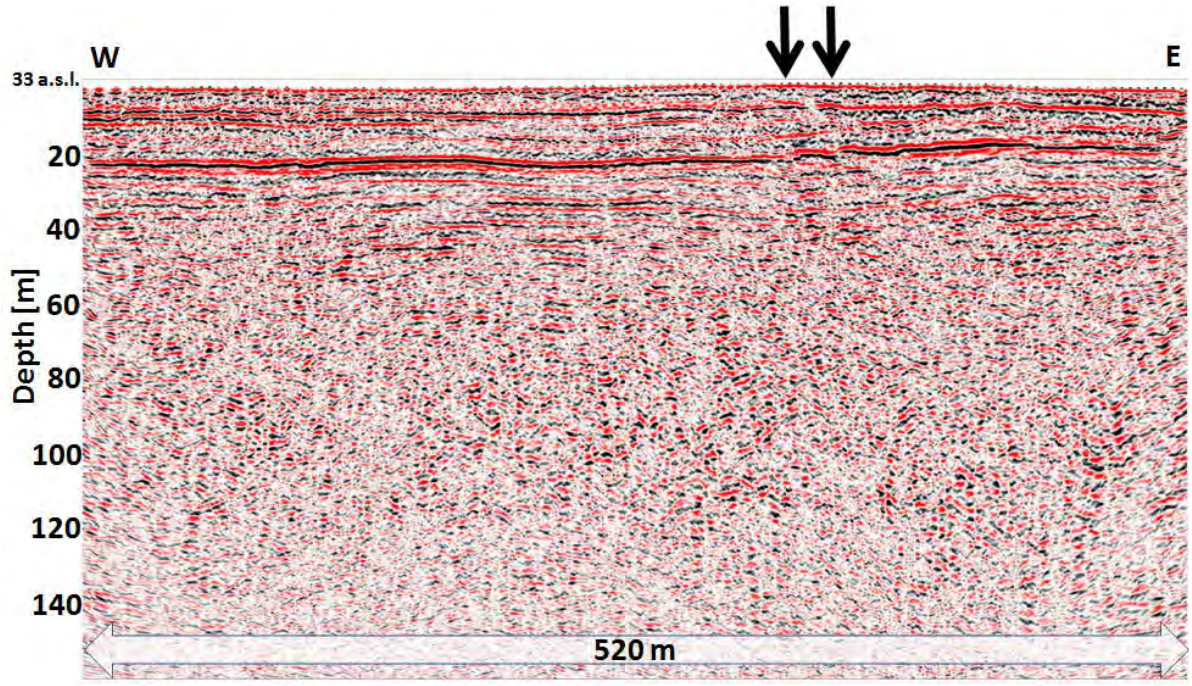

Figure 6.8 Depth converted migrated section of profile 9 along Olympic Drive, Whakatane. This profile is a continuation of profile 8 towards the east, but is offset to the south by 100 m. Note again the continuous reflection of the marker horizon at around 20 m depth, which is only interrupted twice (arrows) by minor vertical offsets. Compared to the discontinuity in the west of profile 8 the structure of the seismic reflectors does not change significantly across this interruption. The vertical offsets could also be associated with faulting, but on a much smaller scale than the main features found in profile 5 and profile 7. Furthermore the features here are restricted to a small depth interval of 20-30 m. See Figure 4.1 for profile location.

We ran a short seismic profile from the eastern end of Goulstone Rd through the pedestrian/river tunnel and up into Gorge Rd (profile 11, see Figure 6.10 and Figure 6.11).

This seismic section is difficult to process since the profile is partly located in a tunnel build of concrete and we had to change the acquisition pattern for the profile. The continuous acquisition pattern as described earlier (see Figure 4.5) had to be split in two sections. Furthermore the profile crosses the border of the soft alluvial sediments in the West to the greywacke basement of the Whakatane Hills in the East, which represents a strong subsurface inhomogeneity affecting the raypaths of the seismic waves. Therefore the imaging results are based on a compromise between the required processing strategies for both lithologies and represent a critical limit for the capabilities of the method.

Figure 6.10 shows the final depth converted and migrated image of the section. We tentatively interpreted the seismic image to show an expected fault location based on the geological data (dashed blue line). It may be indicated by the change in imaged structure and also due to the rapid lateral change in interval velocities (Figure 6.11, dashed pink line). But in fact there are no clear indications of faulting in the seismic image. One reason for the lack of a clearly imaged fault might be that the imaging is affected by the strong lateral variation of the velocity field, which induces smearing effects along the expected contact zone area. A direct comparison with profile 4 shows the marker horizon at 20 m depth in the West of profile 11, which is missing in the Eastern part of profile 11. The location and surface expression of the beginning of the Whakatane Hills is where we expect this horizon to start. It ends where it is interrupted on all remaining profiles further to the West. In summary it must be said that if there is a major fault in this area of the township it is difficult to image and locate with confidence. The results shown here are the best possible seismic images that the method can produce under the given site circumstances.

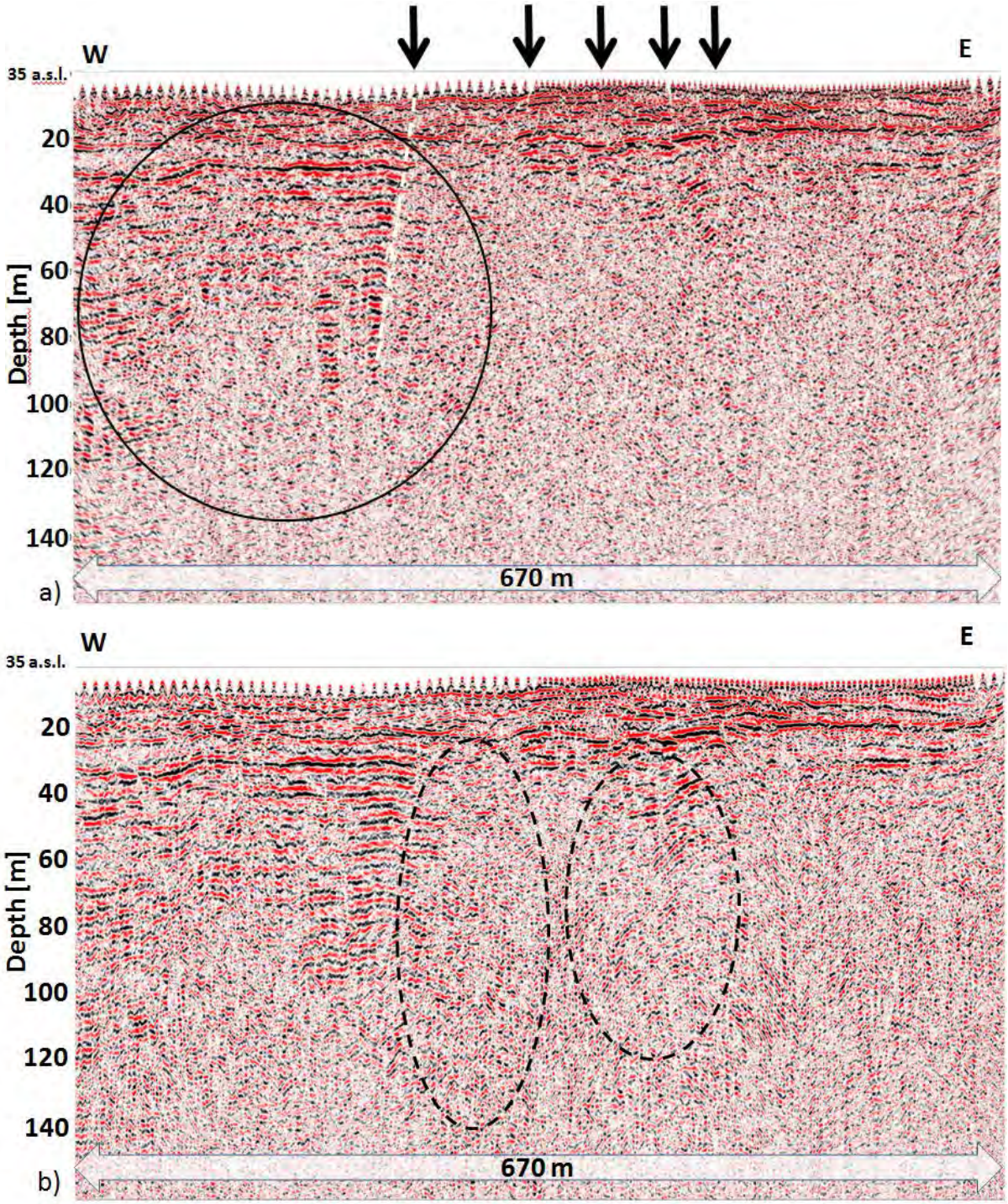

Figure 6.9 a) Depth converted migrated section of profile 10 along Arawa Road, Whakatane. The marker horizon at around 20 m depth is clearly visible but not as continuous as on the previous profiles. It exhibits several steps along the profile (arrows) with one significant interruption (dashed white line) and subsequent change in reflectivity pattern to the West (circled area). b) Non migrated stack section showing strong diffractions (dashed oval areas), which are common fault indicators. These diffractions are removed by the migration process resulting in transparent area in a). See Figure 4.1 for profile location.

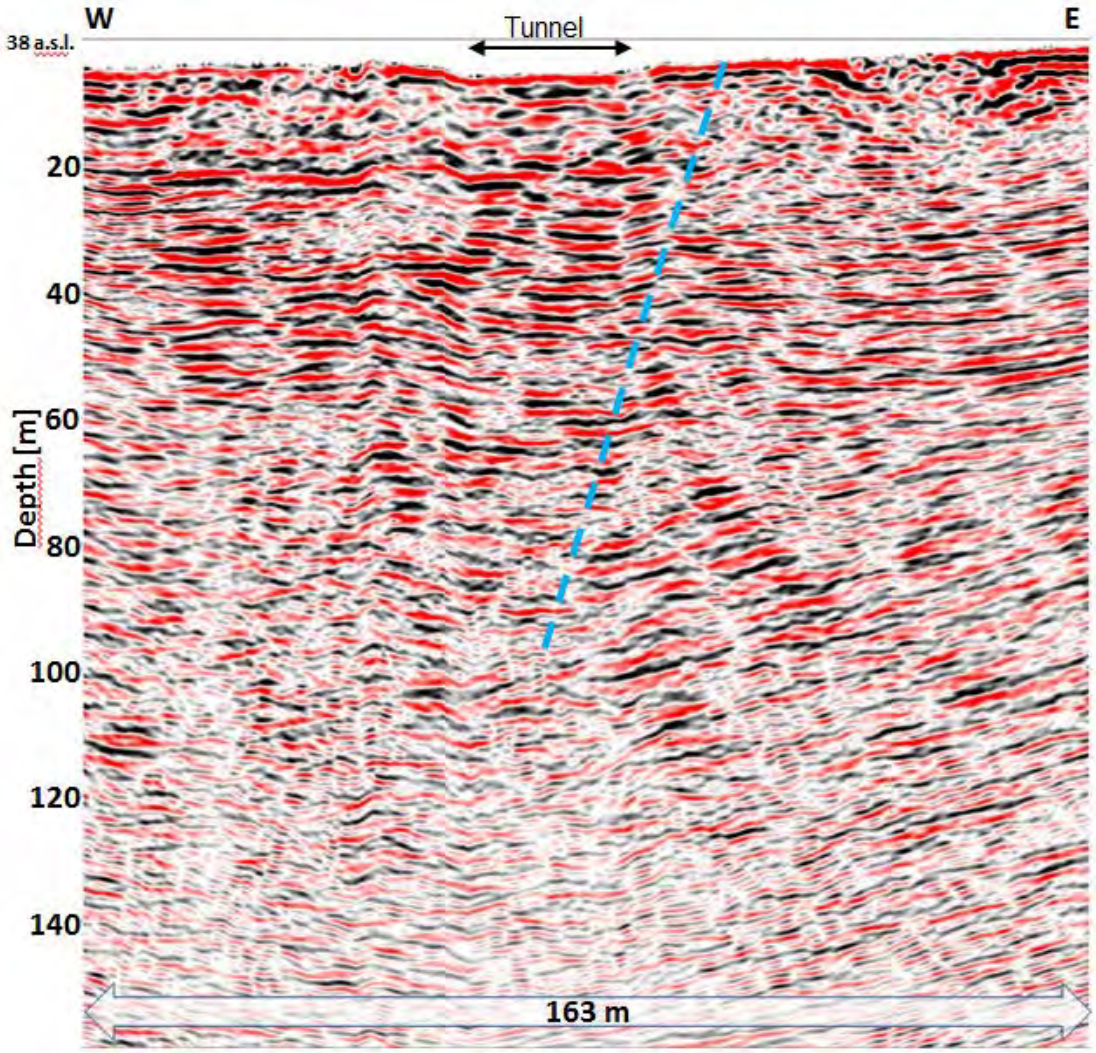

Figure 6.10 Shear wave seismic reflection structure of profile 11 (migrated section). The profile was acquired through the pedestrian tunnel connecting Goulstone Rd and Gorge road, which was an additional challenge, the location of the tunnel is indicated. The dashed blue line gives a tentative interpretation of a potential fault location, which was expected at the contact zone of the soft sediments to the greywacke basement of the Whakatane Hills. But in fact the seismic image shows no clear indications of faulting, and also no clear indications of the contact zone. An imaging of this feature is also affected by the strong lateral variation of the velocity field caused by the geology. Please note the start of the marker horizon nearly 20 m in depth in the West of the profile. The location at the Gorge is where we expect this horizon to start while it ends where it is interrupted on all remaining profiles further to the West. This suggests the location of a fault as indicated.

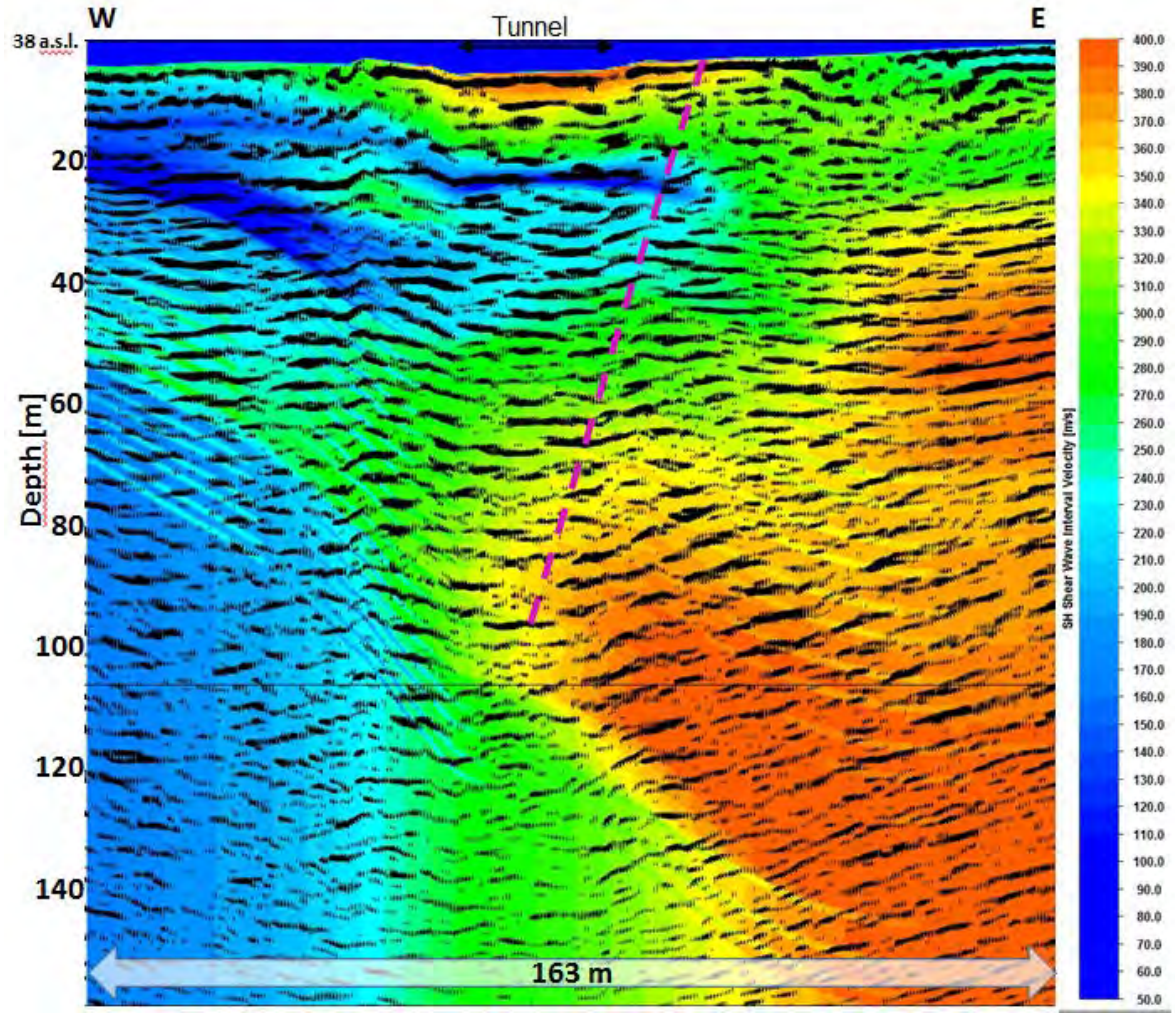

Figure 6.11 Shear wave interval velocity structure for profile 11 (compare with Figure 6.10). The dashed magenta line gives a tentative interpretation of a potential fault location which was expected due to the geological structure. This profile was acquired through the pedestrian tunnel made of concrete connecting Goulstone Rd and Gorge road. The location of the tunnel is indicated and also visible due to the high velocities close to the surface. See Figure 4.1 for profile location.

7.0 DISCUSSION

The present inferred location of the buried fault as represented in the active faults database (Langridge et al., 2016) is marked on Figure 7.1 in purple. Our profiles cross previously expected alignments of the Whakatane Fault in the Whakatane area and we are confident that the fault cuts one or more of the profiles.

Preliminary analysis of the seismic profiles has identified deformation and associated seismic reflector disruption that we infer to represent buried faulting (red and blue markers in Figure 7.1). The most prominent horizon is a widespread sub-horizontal seismic reflector at c. 20 m depth beneath the Whakatane flat land east of Hinemoa Road. This marker horizon is less prominent, disrupted or missing to the west of Hinemoa Road.

The changes in structural features we observe compare well with features identified at, or close to the Edgecumbe Fault that ruptured to the surface in 1987. Four of the fault–related features in Whakatane connect almost along a straight line (yellow line) and we infer that these represent the location of the Whakatane Fault. This change in seismic stratigraphy and structure is recorded in an area where the Whakatane Fault has been inferred to be present. Our preferred Whakatane Fault trace in the Whakatane urban area is located west of the fault as it is currently indicated in the active fault database (purple line in Figure 7.1, Langridge et al., 2016). There is only one location we could identify to show potential active faulting to the east of this line. We do not see significant offsets of seismic horizons or other strong indications for faulting on seismic profiles crossing the inferred Whatakane Fault trace as it is currently given in the active fault database and indicated by the purple line in Figure 7.1.

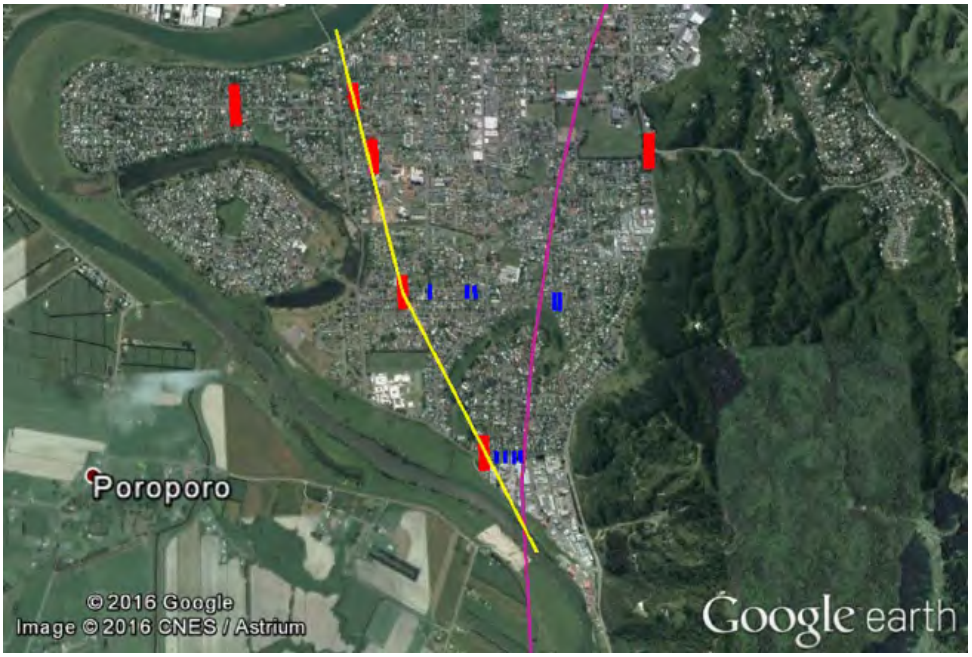

Figure 7.1 Locations of seismic structural features that we connect to potential active faulting (red markers). The blue markers show positions of other small offsets of seismic reflection horizons we've observed in the data. The yellow line connects four of the features observed on individual profiles. The purple line shows the approximated location of the Whakatane fault as it is currently given in the Active Fault Database (Langridge et al., 2016).

Our profiles indicate that the Whakatane Fault through the township is characterised in the subsurface by vertical displacements in the western part of the township. This conclusion is based on observed changes in reflectivity patterns in landstreamer profiles, most clearly by disruption of an otherwise continuous and horizontal 'marker' reflection. We currently correlate this continuous reflection with the interface between marine Holocene and underlying non-marine, dense, silty material found at a depth of nearly 20 m in a recent geological investigation of the Whakatane CBD (Begg et al., 2015).

The yellow line on Figure 7.1 defines a boundary between near-surface continuous and non-continuous seismic reflectors. The location of interruption of the marker horizon coincides with a topographic scarp, stepped in the same sense as the subsurface structure over part of the area, down to the west (Figure 6.6c). To the East of this step Holocene beach ridges are preserved at the surface while to the west, they have been eroded by a small stream and are overlain by silt. Whether this step represents an eroded fault scarp, a river terrace riser or swamp margin that coincides with the location of the changes in reflectivity in the seismic lines requires further investigation (cf. Beetham et al., 2010, Woelz et al., 2010).

South of the Hospital area, no surface expression is visible in photographs, maps or LiDAR. However, the subsurface expression observed on the seismic data is traceable south to Arawa Road. The likely explanation for the lack of surface expression is that the geomorphic surfaces are younger in this area, post-dating the last rupture of the fault.

There are also indications of faulting on profiles crossing the valley outlet at Gorge Road and the western end of James Street (Profile 11 and 6, see Figure 4.1 for location). The nature of these structures would require further investigation and a more detailed interpretation which is beyond the scope of this report.

There are minor displacements of the marker horizon on the east side of the major offsets in the Bridge Street, Olympic Drive and Arawa Road profiles (profiles 8, 9 and 10, Figure 4.1, blue markers in Figure 7.1). These may represent minor splays and based on their apparent vertical offsets are significantly less important than the main structure imaged on several profiles.

Further investigation is required to fully confirm the results of this study and also to finally demonstrate the exact location of the fault. Such investigation could consist of trenching of the potential fault scarp locations and a drilling campaign in the vicinity to the West and East of the yellow line indicated in Figure 7.1 on several of the profiles documented here.

8.0 CONCLUSIONS

Seismic reflection data collected in open greenfield (Edgecumbe Fault) and urban areas (Whakatane Fault) image low Vs sediments in the subsurface of the Rangitikei Plains. The land streamer system, using a shear wave source has proven an excellent method of obtaining subsurface images in these materials and in the difficult environment of urban Whakatane.

Seismic lines across the Edgecumbe Fault were acquired to help understand deformation in subsurface loose sediments across a normal fault with known rupture history. This knowledge has been used to interpret profiles in similar materials within the Whakatane urban area where the location of the inferred northern portion of the Whakatane Fault is uncertain.

Preliminary interpretation of the E-W orientated profiles has located active faulting in the Whakatane urban area. These subsurface locations delineate a fault in a different location to that inferred by Beetham et al. (2010).

This study was focussed on assessing the effectiveness of the land streamer for the purpose of mapping blind faults in an urban environment. More comprehensive interpretation of the data collected during this investigation may confirm the location of subsurface fault-related deformation. Such interpretation will require an understanding of tectonic deformation and sediment architecture in a marine-terrestrial transitional environment, identification of the geological nature and age of prominent reflectors. The landstreamer system helps to identify zones and locations where faulting is potentially occurring and therefore helps to target further geological work.

Earthquakes and fault surface rupture pose a significant hazard to the people, infrastructure and industries of New Zealand and internationally. The ability to routinely map the locations of active faults with geophysical methods within urban environments is a valuable tool for planning and mitigating hazards posed by concealed active faults. Such work will help to build safer communities more resilient to earthquake hazard.

A case can be made for ensuring such a system is routinely available for deployment in New Zealand. Routine application of such an instrument will greatly enhance land use planning, hazard and risk management and earthquake resilience in densely populated communities at comparably low cost. Seismic surveys need to be accompanied by detailed geological and other geophysical investigations to ensure reliable interpretation of results.

9.0 ACKNOWLEDGEMENTS

We thank the New Zealand Earthquake Commission (EQC) for funding this project in New Zealand. We are also very grateful for significant in-kind funding in terms of personnel time and equipment from the Leibniz Institute of Applied Geophysics (LIAG) in Germany. We acknowledge support from GNS Science core funding and overheads. We also thank the Whakatane District Council for logistical support with traffic management and for hosting this study in their district.

10.0 REFERENCES

Aki, K.; Richards, P.G. 1980. Quantitative seismology. W.H. Freeman and Company, San Francisco.

Barrell, D.J.A.; Litchfield, N.J.; Townsend, D.B.; Quigley, M.; Van Dissen, R.J.; Cosgrove, R.; Cox, S.C.; Furlong, K.; Villamor, P.; Begg, J.G.; Hemmings-Sykes, S.; Jongens, R.; Mackenzie, H.; Noble, D.; Stahl, T.; Bilderback, E.; Duffy, B.; Henham, H.; Klahn, A.; Lang, E.M.W.; Moody, L.; Nicol, R.; Pedley, K.; Smith, A. 2011. Strike-slip ground-surface rupture (Greendale Fault) associated with the 4 September 2010 Darfield earthquake, Canterbury, New Zealand. Quarterly Journal of Engineering Geology and Hydrogeology 44, 283-291. doi: 10.1144/1470-9236/11-034.

Beanland, S. 1995. The North Island Dextral Fault Belt, Hikurangi Subduction Margin, New Zealand. PhD Thesis, Victoria, University of Wellington.

Beanland, S.; Berryman, K.R.; Blick, G.H. 1989. Geological investigations of the 1987 Edgecumbe earthquake, New Zealand. New Zealand Journal of Geology and Geophysics 32, 73–91.

Beetham, R.D.; Begg, J.G. 2010. Whakatane Hospital Redevelopment Seismic Fault Analysis. GNS Letter Report No: 2010/171LR. To BECA.

Begg, J.G.; Mouslopoulou, V. 2010. Analysis of late Holocene faulting within an active rift using lidar, Taupo Rift, New Zealand. Journal of Volcanology and Geothermal Research 190, 152–167.

Begg, J.G.; Beetham, R.D.; Ludovic, B.; Nikolaison, H.N. 2015. A 3D geological Model of the Whakatane Central Business District, Bay of Plenty, New Zealand – with estimate maps illustrating possible earthquake land damage. GNS Science Consultancy Report 2015/30, June 2015.

Bexfield, C.E.; McBride, J.H.; Pugin, A.J.M.; Ravat, D.; Biswas, S.; Nelson, W.J.; Larson, T.H.; Sargent, S.L.; Fillerup, M.A.; Tingey, B.E.; Wald, L.; Northcott, M.L.; South, J.V.; Okure, M.S.; Chandler, M.R. 2006. Integration of P- and SH-wave high-resolution seismic reflection and micro-gravity techniques to improve interpretation of shallow subsurface structure: New Madrid seismic zone. Tectonophysics 420, 5-21.

Canterbury Earthquakes Royal Commission, 2012 Volume 1 Summary and Recommendations In Volumes 1-3 Seismicity, Soils And The Seismic Design Of Buildings. 115 p. ISBN: 978-0-478-39558-7

Inazaki T. 2004. High-resolution seismic reflection surveying at paved areas using an S-wave type Land Streamer. Exploration Geophysics 35, 1-6. http://dx.doi.org/10.1071/EG04001.

Crawford, J.M.; Doty, W.; Lee, M.R. 1960. Continuous signal seismograph. Geophysics, 25, 95-105.

Dasios, A.; McCann, C.; Astin, T.; McCann, D.; Fenning, P. 1999. Seismic imaging of the shallow subsurface: Shear wave case histories. Geophysical Prospecting 47, 565-591.

Dix, C.H. 1955. Seismic velocities from surface measurements. Geophysics 20, 68-86.

Ghose, R.; Brouwer, J.; Nijhof, V. 1996. A portable S-wave vibrator for high-resolution imaging of the shallow subsurface. 59th EAGE Conference and Technical Exhibition, Amsterdam, Expanded Abstracts MO37.

Krawczyk, C.M.; Polom U.; Trabs, S.; Dahm, T. 2011. Sinkholes in the city of Hamburg—New urban shear wave reflection seismic system enables high-resolution imaging of subrosion structures. Journal of Applied Geophysics 78, 133-143. ISSN 0926-9851, 10.1016/j.jappgeo.2011.02.003.

Kurahashi, T.; Inazaki, T. 2007. Seismic reflection survey using shear wave vibrator for an active fault. Symposium on the Application of Geophysics to Engineering and Environmental Problems (SAGEEP) 2007. 566-573.

Lamarche, G.; Barnes, P.M.; Bull, J.M. 2006. Faulting and extension rate over the last 20 000 years in the offshore Whakatane Graben, New Zealand continental shelf. Tectonics 25. doi:10.1029/2005TC001886.

Leonard, G.S.; Begg, J.G.; Wilson, C.J.J. (compilers), 2010. Geology of the Rotorua area: scale 1:250,000. Lower Hutt: Institute of Geological & Nuclear Sciences Limited. Institute of Geological & Nuclear Sciences 1:250,000 geological map 5. 99 p. + 1 folded map.

Langridge, R.M.; Ries, W.F.; Litchfield, N.J.; Villamor, P.; Van Dissen, R.J.; Rattenbury, M.S.; Barrell, D.J.A.; Heron, D.W.; Haubrock, S.; Townsend, D.B.; Lee, J.A.; Cox, S.; Berryman, K.R.; Nicol, A.; Stirling, M. 2016. The New Zealand active faults database: NZAFD250. New Zealand Journal of Geology and Geophysics 59(1), 86-96 doi: 10.1080/00288306.2015.1112818.

Malehmir, A.; Zhang, F.; Dehhannejad, M.; Lundberg, E.; Döse, C.; Friberg, O.; Brodic, B.; Place, J.; Svensson, M.; Möller, H. 2015. Planning of urban infrastructure using a broadband seismic landstreamer – Tomography results and uncertainty qualifications from a case study in southwest Sweden. Geophysics 80(6), 177-192.

Mouslopoulou, V.; Nicol, A.; Little, T.A.; Walsh, J.J. 2007. Displacement transfer between intersecting regional strike-slip and extensional fault systems. Journal of Structural Geology 29, 100–116.

Mouslopoulou, V.; Nicol, A.; Walsh, J.J.; Beetham, D.; Stagpoole, V. 2008. Quaternary temporal stability of a regional strike-slip and rift fault intersection. Journal of Structural Geology 30, 451–463.

Mouslopoulou, V.; Nicol, A.; Little, T. A.; Begg, J.G. 2009 Paleoearthquake surface rupture in a transition zone from strike-slip to oblique-normal slip and its implication to seismic hazard, North Island Fault System, New Zealand. In: Historical and Pre-historical Records of Earthquake Ground Effects for Seismic Hazard Assessment. Geological Society, London, Special Publications 316, 269-292 doi:10.1144/SP316.17.

Nairn, I.A. 2002. Geology of the Okataina Volcanic Centre, scale 1:50 000. Institute of Geological and Nuclear Sciences geological map 25.

Nairn, I.A.; Beanland, S. 1989. Geological setting of the 1987 Edgecumbe earthquake, New Zealand. New Zealand Journal of Geology and Geophysics 32, 1–13.

Nicol, A.; Begg, J.; Mouslopoulou, V.; Stirling, M.; Townsend, D.; Van Dissen, R.; Walsh, J. 2011. Active faults in New Zealand: what are we missing? p. 79 In: Litchfield, N.J., Clark, K. (eds). Abstract Volume, Geosciences 2011 Conference, Nelson, New Zealand. Geoscience Society of New Zealand Miscellaneous Publication 130A. ISBN 978-1-877480-13-3.

Omnes, G. 1978. Exploring with SH-Waves. Paper presented at the CSEG national Convention, 1978, Calgary, May 11, 1978. Copyright: CGG, Denver, Colorado 80202.

Polom, U.; Druivenga, G.; Grossmann, E.; Grueneberg, S.; Rode, W. 2011. Transportabler Scherwellenvibrator. Patent application DE 103 27 757 A1, Deutsches Patent- und Markenamt (in German).

Polom, U.; Hansen, L.; Sauvin, G.; L'Heureux, J-S.; Lecomte, I.; Krawczyk, C.M.; Vanneste, M.; Longva, O. 2010. High-resolution SH-wave seismic reflection for characterization of onshore ground conditions in the Trondheim Harbor, central Norway. In Miller, R.D., Bradford, J.H., 700 and Holliger K. 2010: Advances in near-surface seismology and ground-penetrating radar. Geophysical Developments Series, No. 15, 297-312.

Polom, U. 2005. Vibration generator for seismic applications. Patent application US 02005/0102105 A1, USPTO, 12.5.2005.

Polom, U.; Arsyad, I.; Kuempel, H.J. 2008. Shallow shear-wave reflection seismics in the tsunami struck Krueng Aceh River Basin, Sumatra. Advances in Geosciences 14, 135-140.

Pugin, A.J.M.; Larson, T.H.; Sargent, S.L.; McBride, J.H.; Bexfield, C.E. 2004. Near-surface mapping using SH- wave and P-wave seismic land streamer data acquisition in Illinois, US. The Leading Edge (Tulsa, OK), 23(7), 677-682. doi: 10.1190/1.1776740.

Pugin, A.J.M.; Hunter, A.J.; Motazedian, D.; Brooks, G.R.; Kasgin, K.B. 2007. An application of shear wave reflection landstreamer technology to soil response evaluation of earthquake shaking in an urban area, Ottawa, Ontario. Symposium on the Application of Geophysics to Engineering and Environmental Problems (SAGEEP), Environmental and Engineering Geophysics society Annual Meeting, Denver, Colorado, U.S.A., April 1-5.

Pugin, A.J.M.; Brewer, K.; Cartwright, T.; Pullan, S.E.; Didier, H.C.; Hunter, J. 2013. Near surface S-wave seismic reflection profiling – new approaches and insights. First Break 31, 49-60.

Quigley, M.; Villamor, P.; Furlong, K.; Beavan, J.; Van Dissen, R.; Litchfield, N.; Stahl, T.; Duffy, B.; Bilderback, E.; Noble, D.; Barrell, D.; Jongens, R.; Cox, S. 2010a. Previously unknown fault shakes New Zealand's South Island. Eos 91(49), 469-470.

Quigley, M.; Van Dissen, R.; Villamor, P.; Litchfield, N.; Barrell, D.; Furlong, K.; Stahl, T.; Duffy, B.; Bilderback, E.; Noble, D.; Townsend, D.; Begg, J.; Jongens, R.; Ries, W.; Claridge, J.; Klahn, A.; Mackenzie, H.; Smith, A.; Hornblow, S.; Nicol, R.; Cox, S.; Langridge, R.; Pedley, K.; 2010b. Surface rupture of the Greendale Fault during the Darfield (Canterbury) Earthquake, New Zealand: initial findings. Bulletin of the New Zealand Society for Earthquake Engineering 43(4), 236-242.

Quigley, M.; Van Dissen, R.; Litchfield, N.; Villamor, P.; Duffy, B.; Barrell, D.; Furlong, K.; Stahl, T.; Bilderback, E.; Noble, D. 2012. Surface rupture during the 2010 Mw 7.1 Darfield (Canterbury) earthquake: implications for fault rupture dynamics and seismic-hazard analysis. Geology 40(1): 55-58. doi:10.1130/G32528. Woolery, E.W., Street, R., Wang, Z., Harris, J.B., 1993. Near surface deformation in the New Madrid seismic zone as imaged by high-resolution SH-wave seismic methods. Geophysical Research Letters 20, 1615-1618.

Rowland, J.V.; Sibson, R.H. 2001. Extensional fault kinematics within the Taupo Volcanic Zone, New Zealand: soft-linked segmentation of a continental rift system. New Zealand Journal of Geology and Geophysics 44, 271–283.

Taylor, H.; Rowland, J.V.; Dougherty, A.J.; Villamor, P.; Begg, J.G., 2010. GPR and trenching resolve the geometry of the Matata fault zone contributing to the paleoseismic history of the Whakatane Graben. p. 292 IN: Hoskin, P.; Hikuroa, D.; Eccles, J. (conveners) *GeoNZ 2010: geoscience, geothermal: abstract volume: Auckland, 21-24 November 2010.* Wellington: Geoscience Society of New Zealand. Geoscience Society of New Zealand miscellaneous publication 129A.

Taylor, S.K.; Bull, J.M.; Lamarche, G.; Barnes, P.M. 2004. Normal fault growth and linkage in the Whakatane Graben, New Zealand, during the last 1.3 Myr. Journal of Geophysical Research: Solid Earth, 109(B2).

Van Dissen, R.; Barrell, D.; Litchfield, N.; Villamor, P.; Quigley, M.; King, A.; Furlong, K.; Begg, J.; Townsend, D.; Mackenzie, H.; Stahl, T.; Noble, D.; Duffy, B.; Bilderback, E.; Claridge, J.; Klahn, A.; Jongens, R.; Cox, S.; Langridge, R.; Ries, W.; Dhakal, R.; Smith, A.; Hornblow, S.; Nicol, R.; Pedley, K.; Henham, H.; Hunter, R.; Zajac, A.; Mote, T. 2011. Surface rupture displacement on the Greendale Fault during the Mw 7.1 Darfield (Canterbury) earthquake, New Zealand, and its impact on man-made structures. in proceedings. Paper 186, 8 p In: 9th Pacific Conference on Earthquake Engineering, Auckland, New Zealand, 14-16 April, 2011.

Villamor, P.; Berryman, K. 2001. A late Quaternary extension rate in the Taupo Volcanic Zone, New Zealand, derived from fault slip data. New Zealand Journal of Geology and Geophysics 44, 243–269.

Woelz, S.; Beetham, R.D.; Begg, J.G. 2010. Fault assessment by gravity and GPR investigations for a hospital in Whakatane. *In*: Eccles, J.D., Grigor, M.R., Hoskin, P.W.O., Hikuroa, D.C.H. (eds). Abstract Volume, GeoNZ 2010 Conference, Auckland, New Zealand. Geoscience Society of New Zealand Miscellaneous Publication 129A: p.324.

Woodward-Clyde, 1998. Matahina Dam strengthening project. Geological completion report. Unpublished report to ECNZ.

www.gns.cri.nz

Principal Location

1 Fairway Drive
Avalon
PO Box 30368
Lower Hutt
New Zealand
T +64-4-570 1444
F +64-4-570 4600

Other Locations

Dunedin Research Centre
764 Cumberland Street
Private Bag 1930
Dunedin
New Zealand
T +64-3-477 4050
F +64-3-477 5232

Wairakei Research Centre
114 Karetoto Road
Wairakei
Private Bag 2000, Taupo
New Zealand
T +64-7-374 8211
F +64-7-374 8199

National Isotope Centre
30 Gracefield Road
PO Box 31312
Lower Hutt
New Zealand
T +64-4-570 1444
F +64-4-570 4657